

Dark matter detection in the BMSSM

NICOLÁS BERNAL¹, ANDREAS GOUDELIS^{2,3}

¹*Centro de Física Teórica de Partículas (CFTP),
Instituto Superior Técnico, Avenida Rovisco Pais, 1049-001 Lisboa, Portugal*

²*Laboratoire de Physique Théorique d'Orsay, UMR8627-CNRS,
Université Paris-Sud, Bât. 210, F-91405 Orsay Cedex, France*

³*Istituto Nazionale di Fisica Nucleare, Sezione di Padova, I-35131, Padova, Italy*

E-mails: nicolas.bernal@cftp.ist.utl.pt, andreas.goudelis@th.u-psud.fr

Abstract

The addition of non-renormalizable terms involving the Higgs fields to the MSSM (BMSSM) ameliorates the little hierarchy problem of the MSSM. For neutralino dark matter, new regions for which the relic abundance of the LSP is consistent with WMAP (as the bulk region and the stop coannihilation region) are now permitted. In this framework, we analyze in detail the direct dark matter detection prospects in a XENON-like experiment. On the other hand, we study the capability of detecting gamma-rays, antiprotons and positrons produced in the annihilation of neutralino LSPs in the Fermi and oncoming AMS-02 experiments.

Contents

1	Introduction	2
2	The model	3
2.1	Correlated stop-slepton masses	4
2.2	Light stops, heavy sleptons	5
3	‘Detectability’ definition	6
4	Direct detection	7
4.1	Differential event rate	7
4.2	A XENON-like experiment	8
4.3	Results	8
4.3.1	Correlated stop-slepton masses	8
4.3.2	Light stops, heavy sleptons	9
5	Gamma-rays from the Galactic Center	12
5.1	Differential event rate	12
5.2	Modeling the galactic center background	13
5.3	The Fermi experiment	14
5.4	Results	15
5.4.1	Correlated stop-slepton masses	15
5.4.2	Light stops, heavy sleptons	17
6	Positrons	19
6.1	Differential event rate	19
6.2	The background	21
6.3	AMS-02 and positron detection	22
6.4	Results	22
6.4.1	Correlated stop-slepton masses	22
6.4.2	Light stops, heavy sleptons	22
7	Antiprotons	24
7.1	Differential Event Rate	24
7.2	The background	25
7.3	AMS-02 and antiproton detection	25
7.4	Results	26
7.4.1	Correlated stop-slepton masses	26
7.4.2	Light stops, heavy sleptons	27
8	Conclusions	27

1 Introduction

The smallness of the quartic Higgs coupling in the framework of the minimal supersymmetric standard model (MSSM) poses a problem. The tree level bound on the Higgs mass is violated, and large enough loop corrections to satisfy the lower bound on the Higgs mass suggest that the stop sector has rather peculiar features: at least one of the stop mass eigenstates should be rather heavy and/or left-right-stop mixing should be substantial [1].

The situation is different if the quartic Higgs couplings are affected by new physics. If the new physics appears at an energy scale that is somewhat higher than the electroweak breaking scale, then its effects can be parametrized by non-renormalizable terms. The leading non-renormalizable terms that modify the quartic couplings are [2, 3, 4, 5, 6, 7, 8, 9, 10]:

$$W_{\text{BMSSM}} = \frac{\lambda_1}{M}(H_u H_d)^2 + \frac{\lambda_2}{M}\mathcal{Z}(H_u H_d)^2, \quad (1)$$

where \mathcal{Z} is a SUSY-breaking spurion:

$$\mathcal{Z} = \theta^2 m_{\text{susy}}. \quad (2)$$

The first term in equation (1) is supersymmetric, while the second breaks supersymmetry (SUSY). In the scalar potential, the following quartic terms are generated:

$$2\epsilon_1 H_u H_d (H_u^\dagger H_u + H_d^\dagger H_d) + \epsilon_2 (H_u H_d)^2, \quad (3)$$

where

$$\epsilon_1 \equiv \frac{\mu^* \lambda_1}{M}, \quad \epsilon_2 \equiv -\frac{m_{\text{susy}} \lambda_2}{M}. \quad (4)$$

However, let us note that these operators Beyond the MSSM (BMSSM) may destabilize the scalar potential. If $4|\epsilon_1| > \epsilon_2$, the effective quartic coupling along one of the D-flat directions is negative, causing a remote vacuum to form in the presence of which the electroweak vacuum could become metastable [11].

The interplay between the Higgs sector, the stop sector, and the non-renormalizable (NR) operators has interesting consequences for the MSSM baryogenesis [12, 13]. The window for MSSM baryogenesis is extended and, more importantly, can be made significantly more natural. In addition, these operators have implications for yet another cosmological issue, and that is Dark Matter (DM) [14, 15, 13]. The phenomenology of the BMSSM at colliders has been studied in reference [16]; implications for fine-tuning have been analyzed in reference [17].

One of the attractive features of the MSSM is the fact that the lightest R-parity-odd particle (LSP) is a natural candidate for being the dark matter particle. Progress in experimentally constraining the MSSM parameter space restricts, however, the regions where the dark matter is quantitatively accounted for to rather special regions of the MSSM: the focus point region, with surprisingly heavy sfermions; the funnel region, where the mass of the CP-odd neutral Higgs scalar is very close to twice the mass of the LSP; the co-annihilation region, where the mass of the scalar partner of the right-handed tau is very close to the mass of the LSP; and the bulk region, where the bino-LSP and the sleptons are light.

The effects of the NR operators are potentially important for two of these four regions. First, these operators give rise to a new Higgs-Higgs-higgsino-higgsino interaction Lagrangian,

$$-\frac{\epsilon_1}{\mu^*} \left[2(H_u H_d)(\tilde{H}_u \tilde{H}_d) + 2(\tilde{H}_u H_d)(H_u \tilde{H}_d) + (H_u \tilde{H}_d)(H_u \tilde{H}_d) + (\tilde{H}_u H_d)(\tilde{H}_u H_d) \right] + \text{h.c.}, \quad (5)$$

which contributes to the annihilation process of two higgsinos to two Higgs particles. This effect is relevant when the dark matter particle has a significant component of higgsinos, as is the case in the focus point region. Second, as mentioned above, these operators modify the relation between the light Higgs mass and the stop masses. This effect can be important in the bulk region within models where the slepton and stop masses are related, such as the mSUGRA models.

The effect of these operators on the relic density was studied in detail in references [15, 13]. It was found that new regions yielding the correct relic density can arise, especially in the bulk and co-annihilation region. In this work, we examine how the detection prospects of the MSSM are modified by the introduction of terms in equation (3) in the superpotential, focusing ourselves on the re-opened regions.

We shall evaluate the detection perspectives for the main four kinds of detection usually considered in the literature, namely direct detection in a XENON-like experiment, gamma-ray detection from dark matter annihilations in the galactic center for the Fermi mission [18] as well as positron and antiproton detection coming again from dark matter annihilations in the galactic halo and for the oncoming AMS-02 [19] experiment.

2 The model

The BMSSM framework, if relevant to the little hierarchy problem that arises from the lower bound on the Higgs mass, assumes a new physics scale at a few TeV. Since the new degrees of freedom at this scale are not specified, the effect of the new threshold on the running of parameters from a much higher scale cannot be rigorously taken into account. It therefore only makes sense to study the BMSSM effects in a framework specified at low energy. In order to demonstrate some of the most interesting consequences of the BMSSM operators for dark matter, we shall employ the two sets of parameters explored in reference [13]: a model where all sfermion masses are correlated, and a model where the only light sfermions are the stops. The first model demonstrates how the so-called bulk region is re-opened, even for correlated stop and slepton masses. The second model incorporates the interesting process of stop co-annihilation. For both models we focus our attention mainly on regions where the stops are light, since the main motivation for the BMSSM operators is to avoid a heavy stop (which is the cause of the little hierarchy problem). Previous analysis in the context of the MSSM with a light stop was done in references [20, 21].

Within this framework, we calculate the dark matter relic density, and the direct and indirect detection prospects in the presence of the new ϵ_i couplings. We used a modified version of the code `micrOMEGAs` [22, 23], where we implemented the BMSSM Higgs-Higgs-higgsino-higgsino couplings of equation (5), in order to calculate the relic density as well as the cross-sections and decay

channels relevant for dark matter detection. The leading ϵ_i -induced corrections to the spectrum, were implemented using the code `SuSpect` [24].

2.1 Correlated stop-slepton masses

The first scenario considered contains correlated stop and slepton masses, just as the most studied MSSM scenarios, such as the mSUGRA [25, 26, 27, 28] or cMSSM frameworks. In this case, the neutralino LSP is a bino-like state annihilating to the standard model leptons via light slepton exchange. However, this scenario, known as the ‘bulk region’, is highly constrained due to the experimental lower bound on the Higgs mass. In general, in order to fulfill such a constraint either heavy or mixed stops are required [29]. In the BMSSM, nevertheless, it is possible to re-open the bulk region regardless of the structure of the stop sector.

In order to allow for a simple comparison with mSUGRA-models, we focus the attention to the parameters

$$\tan\beta, m_{1/2}, m_0, A_0, \text{sign}(\mu). \quad (6)$$

Let us emphasize again that one should *not* think about this set of parameters as coming from an extended mSUGRA model, since the effects of the BMSSM physics at the few TeV scale on the running are not (and cannot) be taken into account. In addition, we have two extra BMSSM parameters: ϵ_1 and ϵ_2 .

In practice, we make discrete choices of $\tan\beta$, A_0 , $\text{sign}(\mu)$, ϵ_1 and ϵ_2 , and scan over m_0 and $m_{1/2}$. We focus our attention on moderate values of $m_{1/2}$ and m_0 because we are mainly interested in light sfermions and the bulk region. We also use $A_0 = 0$ GeV and $\mu > 0$ in the whole analysis.

As pointed out in reference [13], we would like to emphasize several points regarding the present scenario:

1. A generic point in the former parameter space usually gives rise to a too low annihilation cross-section of neutralino LSP and hence to a too large relic density, in conflict with the WMAP measurements [30].
2. However, for moderate $m_{1/2}$ and low m_0 values, there is a region where the LSP is almost degenerate in mass with the lightest stau ($\tilde{\tau}_1$), enhancing the co-annihilation cross-section $\chi_1^0 - \tilde{\tau}$.
3. Another region giving rise to relic density in agreement with the WMAP measurements appears for $m_{1/2} \sim 120$ GeV. This is the ‘ h -pole’ and the ‘ Z -pole’ region in which $m_h \sim m_Z \sim 2m_{\chi_1^0}$, and the s -channel Higgs and Z boson exchange is nearly resonant, allowing the neutralinos to annihilate efficiently [31]. Let us note that for the ordinary mSUGRA case, this region is already excluded by LEP measurements.
4. For negative enough ϵ_1 values, the uplift of the Higgs mass generates a splitting among the ‘ h -pole’ and the ‘ Z -pole’ regions, with the former now evading LEP constraints.

The latter point concerning the Higgs boson mass is the most significant effect of the BMSSM operators. Within the MSSM with mSUGRA-like correlations, the bound on the Higgs mass strongly constrains $m_{1/2}$. In contrast, in the presence of $\epsilon_1 = \mathcal{O}(-0.1)$, the full region for which the correct value of the relic abundance is obtained is allowed. Let us emphasize that in the plain MSSM scenario at stake the bulk region is already ruled out because it gives rise to a too light Higgs boson, in contradiction to LEP2 data [32]. However, the introduction of the NR operators in equation (1) uplifts the latter mass up to $m_h \gtrsim 130$ GeV or $m_h \gtrsim 155$ GeV for $\tan\beta = 10$ or 3 respectively.

In the m_0 region that we are considering here, the impact of the BMSSM operators on the mass of the neutralino LSP is rather limited. The reason is that in the bulk region the LSP is mostly bino-like, while the BMSSM operators affect the higgsino parameters.

Concerning precision electroweak data and low energy processes, it is important to realize that the new physics that generates the non-renormalizable operators can directly modify the constraints that come from these measurements. Ignoring this point, it is still possible to identify regions in the parameter space favored by the WMAP data which satisfy all such low energy constraints. The relevance of the BMSSM lies in the fact that constraints involving the Higgs are decoupled from constraints involving the stop sector.

2.2 Light stops, heavy sleptons

In order to continue with the analysis of scenarios with light unmixed stops, we focus on a set of low energy parameters very different from the previous subsection. Explicitly, in addition to the BMSSM ϵ_i parameters, we consider the following set of parameters:

$$M_1, \mu, \tan\beta, X_t, m_U, m_Q, m_{\tilde{f}}, m_A, \quad (7)$$

where $m_{\tilde{f}}$ is a common mass for the sleptons, the first and second generation squarks, and \tilde{b}_R . We further use $M_1 = \frac{5}{3} \tan^2\theta_W M_2 \sim \frac{1}{2} M_2$. To demonstrate our main points, we fix the values of all but two parameters as follows: $\epsilon_1 = 0$ or -0.1 , $\epsilon_2 = 0$ or $+0.05$, $\tan\beta = 3$ or 10 , $X_t = 0$, $m_U = 210$ GeV, $m_Q = 400$ GeV, $m_{\tilde{f}} = m_A = 500$ GeV. This scenario gives rise to relatively light stops:

$$m_{\tilde{t}_1} \lesssim 150 \text{ GeV}, \quad 370 \text{ GeV} \lesssim m_{\tilde{t}_2} \lesssim 400 \text{ GeV}. \quad (8)$$

We scan over the remaining two parameters, M_1 and μ .

Again, as pointed out in reference [13], in the prescribed framework one can identify four regions in which the WMAP constraint is fulfilled:

1. The ‘ Z -pole’ region in which the LSP is very light, $m_{\chi_1^0} \sim \frac{1}{2} M_Z \sim 45$ GeV, and the s -channel Z exchange is nearly resonant. This region is not ruled out only in scenarios where the mass splitting between M_1 and M_2 at the electroweak scale is very large.
2. The ‘ h -pole’ region in which the LSP is rather light, $m_{\chi_1^0} \sim \frac{1}{2} M_h$, and the s -channel h exchange is nearly resonant, allowing the neutralinos to annihilate efficiently [31].

3. The ‘mixed region’ in which the LSP is a higgsino–bino mixture [33], $M_1 \sim \mu$, which enhances (but not too much) its annihilation cross-sections into final states containing gauge and/or Higgs bosons: $\chi_1^0 \chi_1^0 \rightarrow W^+ W^-, ZZ, Zh$ and hh .
4. The ‘stop co-annihilation’ region, in which the LSP is almost degenerate in mass with the lightest stop (\tilde{t}_1). Such a scenario leads to an enhanced annihilation of sparticles since the $\chi_1^0 - \tilde{t}_1$ co-annihilation cross-section [34, 35, 36] is much larger than that of the LSP.

Let us first consider the case where $\epsilon_1 = \epsilon_2 = 0$. The region at $M_1 \sim m_Z/2 \sim m_h/2$ corresponds to the s -channel exchange of an almost on-shell Higgs or Z boson. Note that when $2m_{\chi_1^0}$ is too close to the Higgs or Z mass pole, the LSP annihilation is too efficient and leads to a much too small $\Omega_{\text{DM}} h^2$. In any case, for the Higgs mass values obtained here, $m_h \sim 85(98)$ GeV for $\tan \beta = 3(10)$, this region is already excluded by the negative searches for chargino pairs at LEP2 [32].

The region close to $M_2 \sim \mu \sim 200$ GeV corresponds to the LSP being a bino–higgsino mixture with sizeable couplings to W , Z and Higgs bosons, allowing for reasonably large rates for neutralino annihilation into $\chi_1^0 \chi_1^0 \rightarrow W^+ W^-, ZZ, hZ$ and hh final states. Above and below the band, the LSP couplings to the various final states are either too strong or too weak to generate the relevant relic density.

Finally, for larger μ values, the mass of the lightest neutralino approaches the mass of the lightest stop leading to an enhanced co-annihilation cross-section: $\chi_1^0 \tilde{t}_1 \rightarrow W^+ b, gt$ ($\sim 90\%$). Also, to a lesser extent ($\sim 5\%$), the annihilation cross-section of the stop NLSP contributes to the total cross-section by the process $\tilde{t}_1 \tilde{t}_1 \rightarrow gg$.

Next we consider the $\epsilon_1 = -0.1$ case. The features of the DM allowed regions are similar to the previous case. The main difference comes from the important enhancement of the Higgs mass due to the presence of the BMSSM operators. In this case it is possible to disentangle the Z and the h peaks, since the Higgs-related peak moves to higher M_2 values, due to the increase of the Higgs mass: $m_h = 122(150)$ GeV for $\tan \beta = 10(3)$. Furthermore, the latter peak is no longer excluded by chargino searches.

3 ‘Detectability’ definition

Let us now define what we shall be meaning by saying that a certain parameter space point is detectable. We employ a method based on the χ^2 quantity. Consider whichever mode of detection: direct or indirect in any of the three channels (γ -rays, e^+ , \bar{p}) we shall be considering. In all three modes, what is finally measured is a number of events per energy bin. Let us call N_i^{sig} the number of signal (dark matter - induced) events in the i -th bin, the nature of which depends on the specific experiment, N_i^{bkg} the corresponding background events in the same bin, and N_i^{tot} the sum of the two. The variance χ_i^2 in every bin is defined as:

$$\chi_i^2 = \frac{(N_i^{\text{tot}} - N_i^{\text{bkg}})^2}{N_i^{\text{tot}}}. \quad (9)$$

Then, the condition that we impose to characterize a point as detectable, is that at least in one energy bin $\chi_i^2 \gtrsim 5.8$. In Gaussian error terms, this corresponds to a 95% CL.

4 Direct detection

4.1 Differential event rate

In spite of the experimental challenges, a number of efforts worldwide are actively pursuing to directly detect WIMPs with a variety of targets and approaches (for previous works see, e.g. references [37, 38, 39]). Many direct dark matter detection experiments are now either operating or in preparation. All these experiments measure the number N of elastic collisions between WIMPs and target nuclei in a detector, per unit detector mass and per unit of time, as a function of the nuclear recoil energy E_r . The detection rate in a detector depends on the density $\rho_0 \simeq 0.385 \text{ GeV cm}^{-3}$ [40] and velocity distribution $f(v_\chi)$ of WIMPs near the Earth. We assume a Maxwellian halo for WIMP's velocity in the rest frame of our galaxy (for a recent treatment of non-Maxwellian case, see e.g. reference [41]), taking into account the orbital motion of the solar system around the galaxy, and neglecting the motion of the Earth around the Sun [42]:

$$f(v_\chi) = \frac{1}{\sqrt{\pi}} \frac{v_\chi}{1.05 v_0^2} \left[e^{-(v_\chi - 1.05 v_0)^2 / v_0^2} - e^{-(v_\chi + 1.05 v_0)^2 / v_0^2} \right], \quad (10)$$

where $v_0 \simeq 220 \text{ km/s}$ is the orbital speed of the Sun around the galactic center. In general, the differential event rate per unit detector mass and per unit of time can be written as:

$$\frac{dN}{dE_r} = \frac{\sigma_0 \rho_0}{2 m_r^2 m_\chi} F(E_r)^2 \int_{v_{\min}(E_r)}^{\infty} \frac{f(v_\chi)}{v_\chi} dv_\chi, \quad (11)$$

where σ_0 is related to the WIMP-nucleon cross-section, $\sigma_{\chi-p}$, by $\sigma_0 = \sigma_{\chi-p} \cdot (A m_r / M_r)^2$, with $M_r = \frac{m_\chi m_p}{m_\chi + m_p}$ the WIMP-nucleon reduced mass, $m_r = \frac{m_\chi m_N}{m_\chi + m_N}$ the WIMP-nucleus reduced mass, m_χ the WIMP mass, m_N the nucleus mass, and A the atomic weight. F is the nuclear form factor; in the following analysis the Woods-Saxon form factor [43] will be used (a more complete discussion can be found in reference [44]). Let us note that we are assuming identical WIMP-proton and WIMP-neutron cross-sections, and that we are ignoring the spin-dependent interactions. The integration over velocities is limited to those which can give place to a recoil energy E_r , thus there is a minimal velocity given by $v_{\min}(E_r) = \sqrt{\frac{m_N E_r}{2 m_r^2}}$.

A word of caution is also needed here to clarify the results we shall present. As it is obvious from equation (11), the sensitivity of a direct detection experiment depends strongly on the local DM density. The value $\rho_0 \simeq 0.385 \text{ GeV cm}^{-3}$ stated previously, refers to the *overall* density. If DM consists of multiple components, the differential event rate will depend on the *partial* density of the i -th component (along with its velocity distribution).

We already saw that the WMAP constraints can be satisfied in rather restricted regions of the parameter space. So, in most of the parameter space the model's relic density is larger than the Λ CDM one as inferred from WMAP, whereas in some cases it can also become smaller. In the case

$\Omega_{\chi_1^0} h^2 > \Omega_{\text{DM}} h^2$, we can speak of a ‘hard exclusion’ by experimental data, since the predicted relic density cannot be larger than the measured one. But in the case $\Omega_{\chi_1^0} h^2 < \Omega_{\text{DM}} h^2$, things are more complicated. If neutralinos are not enough to explain the total DM relic density, nothing excludes them being only one of the components of the total DM density. In this case, the local density of neutralinos should be renormalised so as to account for this feature. In this sense, when computing whether a parameter space point is detectable or not, we should use the correct local density value (one could assume, for example, that the local density fraction scales as the relic density one).

In the following, we shall be ignoring this point. We shall be computing sensitivity lines considering the local density as being constant over the parameter space. In this spirit, the sensitivity lines should be read with a little caution. They can be read safely with respect to the regions where both WMAP bounds are fulfilled (the upper and the lower), whereas the reader should keep the previous remarks in mind for the bulk of the parameter space. When we say that a region of the parameter space is detectable, this corresponds literally to the WMAP fully compatible regions.

4.2 A XENON-like experiment

The XENON experiment aims at the direct detection of dark matter via its elastic scattering off xenon nuclei. It allows the simultaneous measurement of direct scintillation in the liquid and of ionization, via proportional scintillation in the gas. In this way, XENON discriminates signal from background for a nuclear recoil energy as small as 4.5 keV. Currently, the collaboration is working with a 170 kg detector, but the final project is a machine containing 1 ton of xenon.

In our study, following reference [45] we will always consider 7 energy bins between 4 and 30 keV. We could take into account non-zero background using simulations of the recoil spectra of neutrons in our analysis, and this would significantly degrade the sensitivity of the detector. However, this would involve a much more detailed study of the detector components (shielding, etc.), and we will not carry it out. In that sense, our results will be the most optimistic ones. Comprehensive studies about the influence of astrophysical and background assumptions can be found in references [46, 47]. Furthermore, we examine three ‘benchmark’ experimental setups, assuming exposures $\varepsilon = 30, 300$ and 3000 kg-year, which could correspond e.g. to a detector with 1 ton of xenon and 11 days, 4 months or 3 years of data acquisition, respectively.

Let us note that other promising direct dark matter detection experiments such as SuperCDMS [48] and LUX [49], should give rise to sensitivities comparable to XENON’s one.

4.3 Results

4.3.1 Correlated stop-slepton masses

Figure 1 shows the exclusion lines (black lines) for exposures $\varepsilon = 30, 300$ and 3000 kg-year, on the $[m_0, m_{1/2}]$ parameter space, for all other parameters as defined in section 2.1. The first-row plots correspond to plain mSUGRA scenarios whereas the second and third to the ‘mSUGRA-like’ benchmark, with the ϵ_1 and (ϵ_1, ϵ_2) parameters turned on respectively. The plots on the left correspond to a choice $\tan\beta = 3$ whereas the right-hand side ones to $\tan\beta = 10$. These curves

reflect the XENON sensitivity and represent its ability to test and exclude different regions of the mSUGRA and BMSSM relevant model at 95% CL: all points lying below the lines are detectable. We note that when some line is absent, this means that the whole parameter space can be probed for the corresponding exposure. Furthermore, the regions in orange (light gray) or blue (dark gray) are excluded due to the fact that the LSP is the stau or because of the null searches for charginos and sleptons at LEP. For large $\tan\beta$, an important fraction of the $[m_0, m_{1/2}]$ plane, corresponding to the region above the violet line, generates an unstable vacuum and is then excluded. Let us note that the introduction of ϵ_2 alleviates the vacuum stability constraint [11], and slightly increases the Higgs mass.

As a general rule, the detection prospects are maximised for low values of the m_0 and $m_{1/2}$ parameters. For higher m_0 values, the masses of the squarks in the internal propagators increase, penalising the scattering cross-section. In the same way, the increase of $m_{1/2}$ augments the WIMP mass and leads to a deterioration of the detection perspectives. On the other hand, the region of low $m_{1/2}$ is also preferred because in that case the lightest neutralino is a mixed bino-higgsino state, favouring the $\chi_1^0 - \chi_1^0 - h$ and $\chi_1^0 - \chi_1^0 - H$ couplings, and therefore the scattering cross-section. Let us recall that a pure higgsino or a pure gaugino state does not couple to the Higgs bosons. On the other hand, the detection prospects are also maximised for low values of $\tan\beta$. For large values, besides the increase of the lightest Higgs boson mass, the coupling of the latter to a χ_1^0 pair decreases significantly because it is proportional to $\sin 2\beta$, for $|\mu| \gg M_1$.

The introduction of the NR operators gives rise to an important deterioration of the detection prospects. The main effect enters via the important increase in the lightest CP-even Higgs mass. This behavior is attenuated for larger values of $\tan\beta$; the corrections to the Higgs masses being suppressed by $1/\tan\beta$ (see e.g. reference [7]). Moreover, as in the bulk region the lightest neutralino is mostly a bino-like state, the impact on its couplings with Higgs bosons is marginal. Nevertheless, let us emphasize again that this deterioration is relative, since we are comparing with a plain MSSM, which is already excluded because of the light Higgs mass.

Concerning the plots in figure 1, a further remark that can be made is that, even for low exposures, a sizable amount of the parameter space can be probed. The experiment will be particularly sensible to low values of $m_{1/2}$. However, larger exposures could be able to explore almost the whole parameter space taken into account. Let us emphasize that, in general terms, the best detection prospects correspond to low values for $\tan\beta$ and for the couplings ϵ_i .

4.3.2 Light stops, heavy sleptons

Figure 2 shows the exclusion lines for XENON with exposures $\varepsilon = 30, 300$ and 3000 kg·year, on the $[M_1, \mu]$ parameter space, with the other parameters as defined in section 2.2 for $\tan\beta = 3$ (left panel) and 10 (right panel). Here again, the experiment will be sensitive to the regions below the contours. It can be seen that, in general, the detection prospects are maximised for low values for the M_1 and/or the μ parameters, corresponding to a light χ_1^0 . On the other hand, the scattering cross-section is enhanced near the region $M_1 \sim \mu$, where the lightest neutralino is a mixed bino-higgsino state, favouring the $\chi_1^0 - \chi_1^0 - h$ and $\chi_1^0 - \chi_1^0 - H$ couplings. Again, the detection prospects

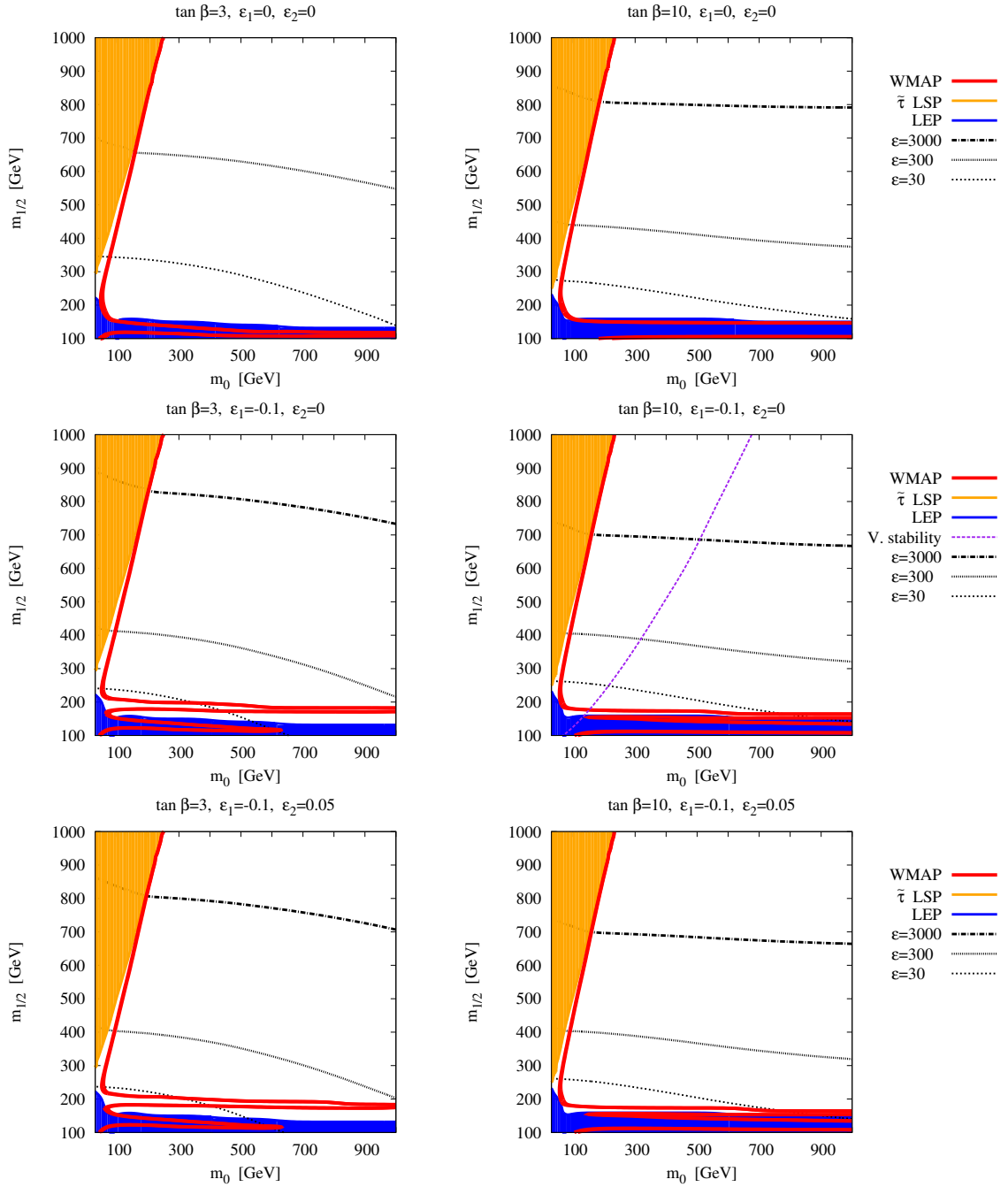


Figure 1: Regions in the $[m_0, m_{1/2}]$ plane that can be detected by XENON using exposures $\varepsilon = 30, 300$ and 3000 kg-year, for our mSUGRA-like scenario. The black lines depict the detectability regions: the area below the lines can be probed. Whenever a line is absent, this means that the whole parameter space can be tested by the experiment. The blue and orange regions depict the areas that are excluded by direct LEP chargino searches and the requirement for a neutralino LSP respectively. The area above the violet line is excluded by the metastable vacuum constraint.

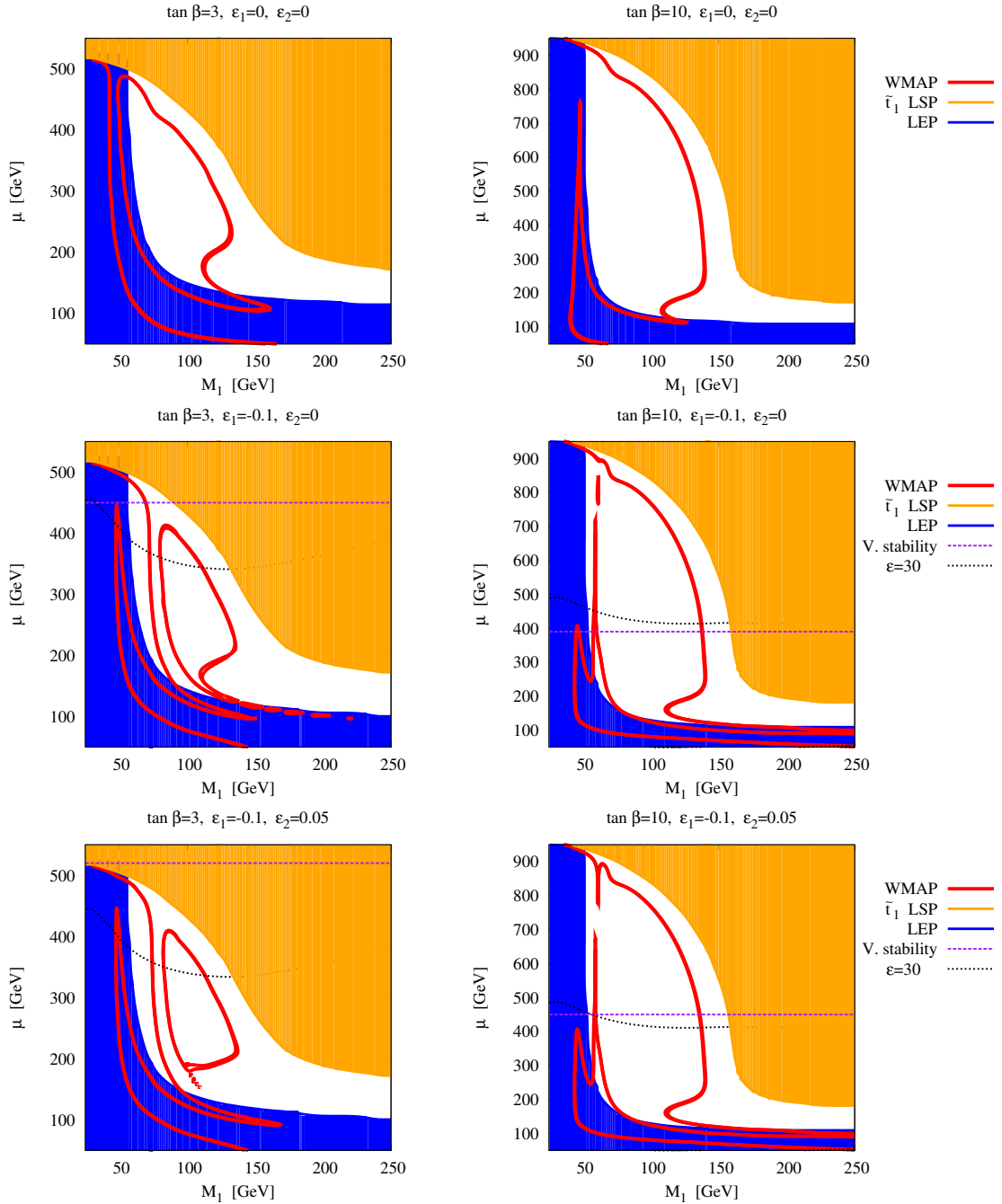


Figure 2: Regions in the $[M_1, \mu]$ plane that can be detected by XENON for the scenario with light stops and heavy sleptons. The black lines depict the detectability regions for the corresponding XENON detector with exposures $\varepsilon = 30, 300$ and 3000 kg-year: the area below the lines can be probed. Whenever a line is absent, this means that the whole parameter space can be tested by the experiment. The blue and orange regions depict the areas that are excluded by direct LEP chargino searches and the requirement for a neutralino LSP respectively. The areas above the violet lines are excluded by the metastable vacuum constraints.

are also improved for low values of $\tan\beta$, mostly because the coupling between the LSP and the Higgs bosons is suppressed by the factor $\sin 2\beta$, for $|\mu| \gg M_1$. Let us note that the first line of the figure (corresponding to the case without the NR operators), besides being excluded by the Higgs mass, is partially ruled out by XENON10 [45] and CDMS [50] searches.

When introducing the dimension 5 operators the detection prospects deteriorate, in a similar way as in the last subsection, because of the rise of the lightest Higgs mass. Furthermore, because of a suppression of the $\chi_1^0 - \chi_1^0 - h$ coupling. The latter effect is very accentuated in the region where the LSP is higgsino-like. It is interesting however to notice that, for the case of large $\tan\beta$, almost the whole area that could not be tested for $\varepsilon = 30$ kg·year is already excluded by the vacuum stability constraint (i.e. the region above the violet line). Moreover, in this case the whole parameter space evades the current constraints from direct detection.

Let us emphasise that this scenario offers moreover exceptionally good detection perspectives. Even with middle exposures, XENON will be able to detect dark matter in the whole region for all three benchmarks and in the two models.

5 Gamma-rays from the Galactic Center

5.1 Differential event rate

The differential flux of gamma-rays generated from dark matter annihilations and coming from a direction forming an angle ψ with respect to the galactic center (GC) is

$$\frac{d\Phi_\gamma}{dE_\gamma}(E_\gamma, \psi) = \frac{\langle\sigma v\rangle}{8\pi m_\chi^2} \sum_i \frac{dN_\gamma^i}{dE_\gamma} Br_i \int_{\text{line of sight}} \rho(r)^2 dl \quad (12)$$

where the discrete sum is over all dark matter annihilation channels, dN_γ^i/dE_γ is the differential gamma-ray yield of SM particles into photons, $\langle\sigma v\rangle$ is the total self-annihilation cross-section averaged over its velocity distribution, ρ is the dark matter density profile, r is the distance from the GC and Br_i is the branching ratio of annihilation into the i -th final state. The decay of SM particles into gammas has been calculated with PYTHIA [51]. The integration is performed along the line of sight from the observation point towards the GC.

It is customary to rewrite equation (12) introducing the dimensionless quantity J , which depends only on the dark matter distribution (for an explicit calculation see, e.g.[52, 53]):

$$J(\psi) = \frac{1}{R_0 \rho_0^2} \int_{\text{line of sight}} \rho(r(l, \psi))^2 dl, \quad (13)$$

where $R_0 \sim 8.5$ kpc is the distance from the Sun to the GC. After having averaged over a solid angle, $\Delta\Omega$, the gamma-ray flux can now be expressed as

$$\begin{aligned} \Phi_\gamma(E_\gamma) &= 1.55 \cdot 10^{-13} \text{ cm}^{-2} \text{ s}^{-1} \text{ GeV}^{-1} \text{ sr}^{-1} \\ &\cdot \sum_i \frac{dN_\gamma^i}{dE_\gamma} \left(\frac{Br_i \langle\sigma v\rangle}{10^{-29} \text{ cm}^3 \text{ s}^{-1}} \right) \left(\frac{100 \text{ GeV}}{m_\chi} \right)^2 \bar{J}(\Delta\Omega) \Delta\Omega. \end{aligned} \quad (14)$$

The value of $\overline{\mathcal{J}}(\Delta\Omega)\Delta\Omega$ depends crucially on the dark matter distribution. There are various ways to parametrize the density profile [54, 55, 56]. The most usual one is

$$\rho(r) = \frac{\rho_0 [1 + (R_0/a)^\alpha]^{(\beta-\gamma)/\alpha}}{(r/R_0)^\gamma [1 + (r/a)^\alpha]^{(\beta-\gamma)/\alpha}}, \quad (15)$$

where a is a characteristic length.

There has been quite some controversy on the values for the (α, β, γ) parameters. Some N-body simulations suggested highly cusped inner regions for the galactic halo [57], whereas others predicted more moderate γ values (the basic parameter determining the inner slope of the profile) [58]. The recent Via Lactea II simulation [59] seems to partly verify earlier results by Navarro *et al.* and finds their results as being well reproduced by $(\alpha, \beta, \gamma) = (1, 3, 1)$. On the other hand, the Aquarius project simulation results [60] seem to be better reproduced by a different parametrization, the so-called Einasto profile [61]:

$$\rho(r) = \rho_s \exp \left[-\frac{2}{\alpha} \left(\left(\frac{r}{r_s} \right)^\alpha - 1 \right) \right], \quad \alpha = 0.17, \quad (16)$$

which does not demonstrate this effect of cuspyness in the inner galactic region. Here $r_s = 20$ kpc is a characteristic length, while ρ_s is a normalization factor, which we fix so as to reproduce the solar dark matter density. This choice yields $\rho_s \approx 0.0783$ GeV cm⁻³.

In most numerical simulations, among which the Via Lactea II and Aquarius, it is a common simplification that the effect of baryons is not taken into account. It has however been pointed out that in the presence of baryons there can be adiabatic collapse phenomena taking place near the galactic center (see, e.g. references [62, 63]), something which could severely influence the innermost regions of the DM halo, leading to profiles much more cusped than the ones usually predicted, and hence enhancing the relevant fluxes by important factors. We thus also consider a profile which, starting from the NFW one, tries to take into account such effects, leading to an enhanced inner slope; this profile with adiabatic compression is denoted NFW_c. The parameters relevant for the models under discussion can be seen in table 1.

It is worth noticing here that we are neglecting the effect of clumpiness, even though other studies showed that, depending upon assumptions on the clumps' distribution, in principle an enhancement by a factor 2 to 10 is possible [64, 59]. In this respect, the following predictions on the gamma-ray flux from the galactic center are conservative. This shall also be the case in the following analysis regarding the detection capacity of the model in the positron and antiproton channels.

As a final remark, let us repeat the word of caution already mentioned for direct detection. In order to draw sensitivity lines, we shall be considering a one-particle DM with the aforementioned density profiles irrespectively of the relic density inferred from the model. Hence, once again, these lines should be read with respect to the WMAP-compatible regions.

5.2 Modeling the galactic center background

HESS [65] has measured the gamma-ray spectrum of a very bright point-like source very close to the galactic center in the range of energy $\sim [160$ GeV–10 TeV]. The collaboration claims that the

	a [kpc]	α	β	γ	$\bar{J}(3 \cdot 10^{-5} \text{ sr})$
Einasto	-	-	-	-	$6.07 \cdot 10^3$
NFW	20	1.0	3.0	1.0	$8.29 \cdot 10^3$
NFW _c	20	0.8	2.7	1.45	$5.73 \cdot 10^6$

Table 1: Einasto, NFW and NFW_c density profiles with the corresponding parameters, and values of $\bar{J}(\Delta\Omega)$. The latter has been computed by means of a VEGAS Monte-Carlo integration algorithm, imposing a constant density for $r \leq 10^{-7}$ kpc so as to avoid divergences appearing in the NFW-like profiles.

data are fitted by a power-law

$$\phi_{\text{bkg}}^{\text{HESS}}(E) = F_0 E_{\text{TeV}}^{-\alpha}, \quad (17)$$

with a spectral index $\alpha = 2.21 \pm 0.09$ and $F_0 = (2.50 \pm 0.21) \cdot 10^{-8} \text{ m}^{-2} \text{ s}^{-1} \text{ TeV}^{-1}$. The data were taken during the second phase of measurements (July–August, 2003) with a χ^2 of 0.6 per degree of freedom. Because of the constant slope power-law observed by HESS, it turns out possible but difficult to conciliate such a spectrum with a signal from dark matter annihilation [63, 66]. Indeed, final particles (quarks, leptons or gauge bosons) produced through annihilations give rise to a spectrum with a continuously changing slope. Several astrophysical models have been proposed in order to match the HESS data [67]. In the present study we consider the astrophysical background for gamma-ray detection as the one extrapolated from the HESS data with a continuous power-law over the energy range of interest ($\approx 1 - 300$ GeV).

EGRET [68] reported the presence of a bright gamma-ray source at energies below 10 GeV, which exceeds by far the HESS aforementioned extrapolation. However, this source seems not to be confirmed by the recent Fermi collaboration data [69]. We shall hence not take into account this point source.

Finally, we will consider the diffuse background of gamma rays in the region surrounding the galactic center. We will describe the spectrum of the background using the HESS observation from the Galactic Center Ridge [70], which can be described by

$$\phi_{\text{bkg}}^{\text{diff}}(E) = 1.1 \cdot 10^{-4} E_{\text{GeV}}^{-2.29} \text{ GeV}^{-1} \text{ cm}^{-2} \text{ s}^{-1} \text{ sr}^{-1}. \quad (18)$$

In our analysis, we shall consider a solid angle of observation around the galactic center ($\Delta\Omega = 3 \cdot 10^{-5}$ sr) and the energy region between 1 and 300 GeV.

5.3 The Fermi experiment

The space-based gamma-ray telescope Fermi [71, 72] was launched in June 2008 for a five-year mission. It performs an all-sky survey covering a large energy range (≈ 30 MeV – 300 GeV). With an effective area and angular resolution on the order of 10^4 cm^2 and 0.1° ($\Delta\Omega \sim 3 \cdot 10^{-5}$ sr) respectively, Fermi will be able to point and analyze the inner center of the Milky Way (~ 7 pc). Concerning the requested condition on the χ^2 for a signal discovery, we have used an analysis similar to the one considered in the case of direct detection as defined in section 3. Additionally,

we take into account a five-year mission run, and an energy range extending up to 300 GeV, with 20 logarithmically evenly spaced bins.

5.4 Results

5.4.1 Correlated stop-slepton masses

In figure 3 we present the detectability regions for a 5-year run of the Fermi experiment and for 3 different halo profiles presented in the literature, Einasto, NFW and NFW_c, in the $[m_0, m_{1/2}]$ parameter space. Fermi will be sensitive to the regions below the contours and, for $\tan\beta = 3$, to the area inside the blob. The detection prospects are maximised for low values of the m_0 and $m_{1/2}$ parameters. For higher m_0 values, the masses of the squarks increase, penalising the annihilation cross-section. However, the growth of $m_{1/2}$ gives rise to the opening of some relevant production channels, after passing some thresholds, increasing significantly the $\langle\sigma v\rangle$. The first one corresponds to a light neutralino, with mass $m_\chi \sim m_Z/2$ ($m_{1/2} \sim 130$ GeV). In that case the annihilation is done via the s -channel exchange of a real Z boson, decaying in hadrons ($\sim 70\%$), neutrinos ($\sim 20\%$) and charged leptons ($\sim 10\%$). The second threshold appears for $m_\chi \sim m_W$ ($m_{1/2} \sim 220$ GeV). The annihilation cross-section is enhanced by the opening of the production channel of two real W^\pm bosons in the final state. This process takes place solely through chargino exchange, since both Z and Higgs bosons exchange are suppressed by taking the limit $v \rightarrow 0$. The last threshold corresponds to the opening of the channel $\chi_1^0\chi_1^0 \rightarrow t\bar{t}$ ($m_{1/2} \sim 400$ GeV). The diagrams involved in such a process contain contributions from t - and u -channel exchange of stops, and from s -channel exchange of Z 's and pseudoscalar Higgs bosons. The aforementioned threshold appears as a particular feature on the left-hand side plots: An isolated detectable region for $m_{1/2} \sim 400$ -500 GeV and $m_0 \lesssim 300$ GeV corresponding to the annihilation into a pair of real top quarks.

Larger values for the annihilation cross-section can be reached for higher values of $\tan\beta$. In that case, the production process of a pair of down-type quarks (in particular $b\bar{b}$ pairs) and charged leptons, dominates the total cross-section. In fact, the diagrams containing exchanges of a pseudoscalar Higgs boson or a sfermion are enhanced by factors $\tan\beta$ and $1/\cos\beta$ respectively. On the other hand, for high values of $\tan\beta$, the channels corresponding to the annihilations into W^+W^- and $t\bar{t}$ vanish. The first because of the reduction of the coupling $\chi_1^0 - \chi_i^\pm - W^\mp$; the second because of important destructive interference between diagrams containing the exchange of a Z boson and stops.

For the present scenario, the introduction of the NR operators gives rise to a very mild signature. Actually, as in almost the whole parameter space the lightest neutralino is bino-like, its couplings do not vary drastically. Moreover, the increment in the Higgs masses has a small impact on the $\langle\sigma v\rangle$ factor. For indirect detection prospects, the main effect corresponds to a slight increase in the LSP mass. Let us emphasize on the fact that, however, the detectable regions are in the BMSSM case more cosmologically relevant than in the corresponding plain MSSM one.

Concerning figure 3, let us note that the only astrophysical setup in which some useful information can be extracted is the NFW_c one. This means that in this scenario, in order to have some positive detection in the γ -ray channel, there should exist some important enhancement of

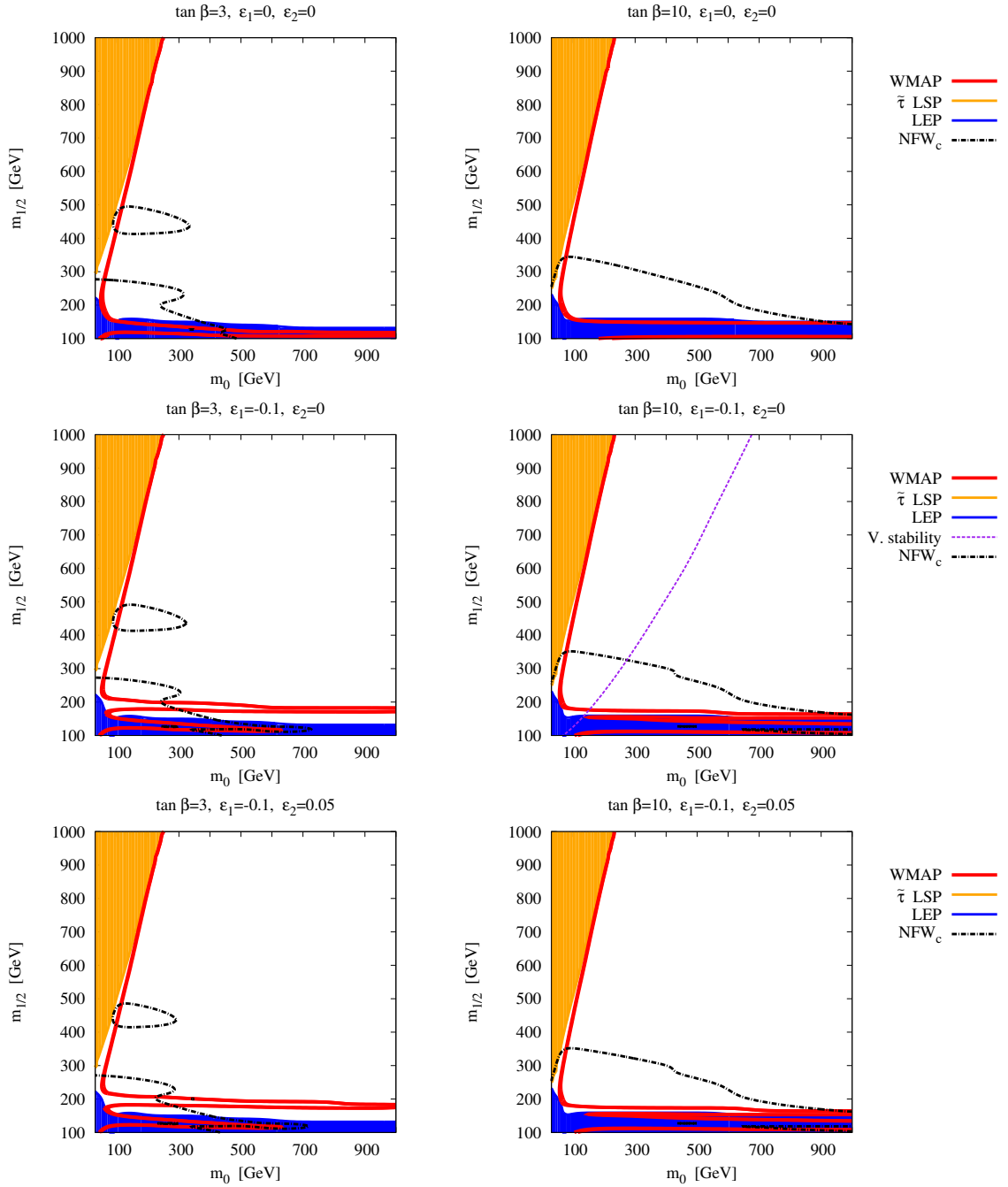


Figure 3: Regions in the $[m_0, m_{1/2}]$ plane that can be detected by the Fermi satellite mission for our mSUGRA-like scenario. The black lines depict the detectability regions for the corresponding halo profile assumptions and 5 years of data acquisition: the area below and on the left of the lines can be probed. The same applies to the top-resonance blob at $m_{1/2} \sim 450$ GeV appearing on the left-hand side plots. For NFW and Einasto profiles, the model could not be tested.

the signal by some astrophysical mechanism (as the adiabatic contraction mechanism invoked in this case). We note that, and this will be different from the case of antimatter signals, there is however no important constraint on astrophysical boosts from the Galactic Center. Gamma-ray detection does not rely, as is the case for positrons that we shall examine in section 6, that much on local phenomena. In this respect, the NFW_c results can be characterized as optimistic (it has been pointed out that even by changing the gravitational collapse conditions, the results can get even more pessimistic in the case, e.g., of a binary black hole formation in the GC), but not excluded.

5.4.2 Light stops, heavy sleptons

Figure 4 presents the results for the second scenario with light stops and heavy sleptons. The experiment will be sensitive to the regions below/on the right of the contours. Again, the detection prospects are maximised for low values of the M_1 and μ parameters, corresponding to light WIMPs. However, the growth of any of the latter parameters gives rise to the opening of some production channels, enhancing significantly the $\langle\sigma v\rangle$. The first one appears for $m_\chi \sim m_Z/2$ and corresponds to the s -channel exchange of a real Z boson. The second one concerns the production channel of two real W bosons. Let us note that in this scenario the neutralino LSP can be as heavy as ~ 110 GeV, implying that the annihilation into a pair of top quarks is never kinematically allowed. On the other hand, the region where $M_1 \gg \mu$ is highly favored for indirect detection due to the fact that the LSP is higgsino-like, maximising its coupling to the Z boson. Let us recall that the Z boson does not couple to a pure gaugino-like neutralino.

Large values for the annihilation cross-section can be reached for high values of $\tan\beta$, mainly because of the enhanced production of $b\bar{b}$ pairs. On the other hand, for high values of $\tan\beta$, the threshold corresponding to the opening of the annihilation into W^+W^- is suppressed or enhanced for $\mu \gg M_1$ or $\mu \ll M_1$ respectively, due to the dependence of the $\chi_1^0 - \chi_i^\pm - W^\mp$ coupling on the texture of the LSP.

For the present scenario, the introduction of the NR operators gives rise to an important increase of the $\chi_1^0 - \chi_1^0 - A$ coupling when $\mu > M_1$, and therefore to a boost in the annihilation into fermion pairs. On the other hand, as the Higgs boson h becomes heavier, the processes giving rise to the final state hZ get kinematically closed.

In the case presented in figure 4, there is a positive detection for all three halo profiles; however, the regions that can be probed for either the NFW or the Einasto cases are cosmologically irrelevant.

In fact, they could give rise to a positive detection near the Z -funnel and in the region where the LSP is a higgsino state ($M_1 \gtrsim 150$ GeV); nevertheless the first is already excluded by LEP (at least for minimal scenarios) and the second generates too small a dark matter relic density, below the WMAP limits. On the other hand, the profile NFW_c could test a large amount of the parameter space we examine, particularly for high values of $\tan\beta$. Only the Higgs peak and the regions with a heavy LSP escape from detection.

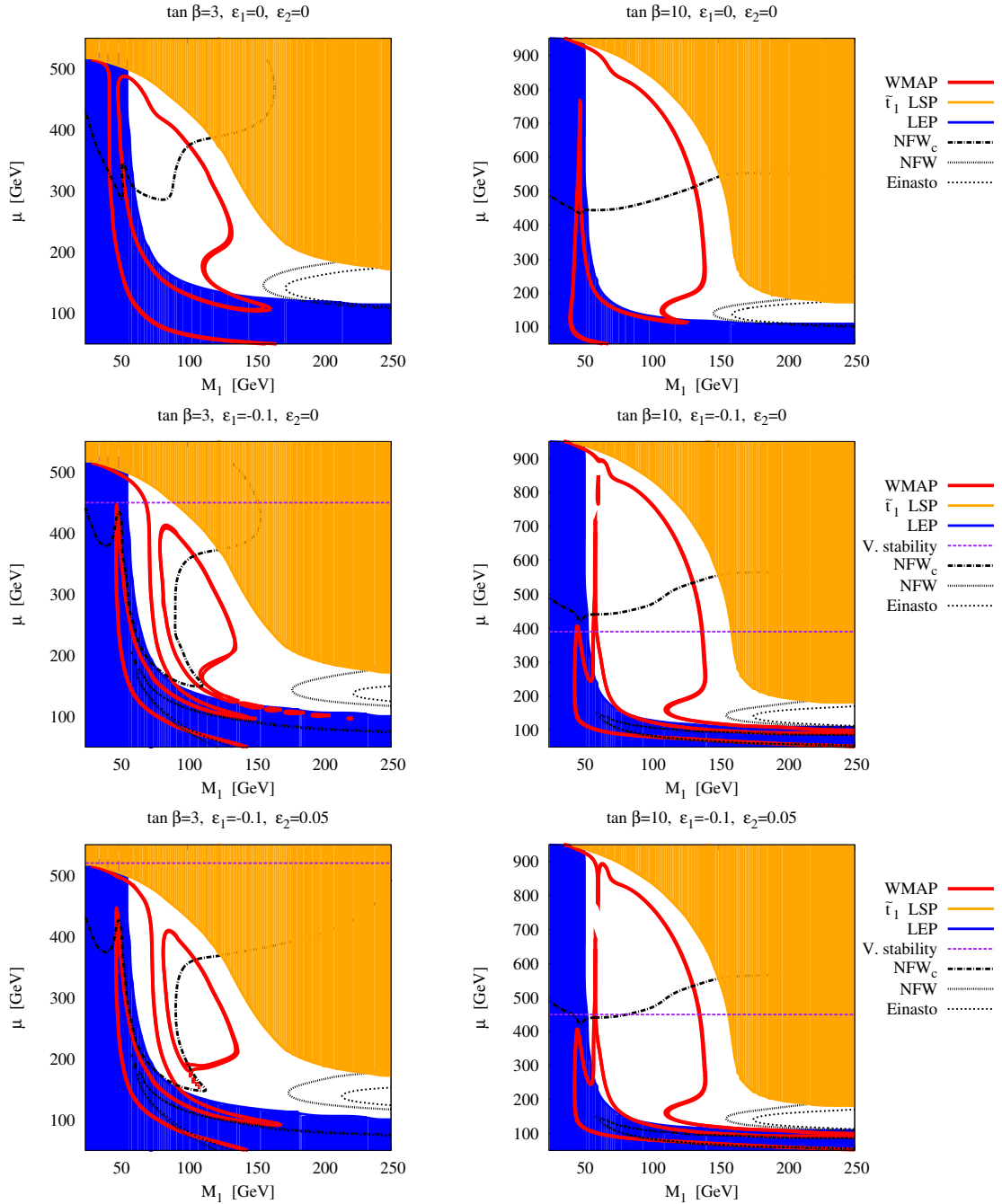


Figure 4: Regions in the $[M_1, \mu]$ plane that can be detected by the Fermi satellite mission for our scenario with light stops and heavy sleptons. The black lines depict the detectability regions for the corresponding halo profile assumptions and 5 years of data acquisition: the area below the lines can be probed. The same applies to lines forming closed regions with respect to the axes, as is the case for the NFW and NFW_c profiles: the parameter space points lying in the interior of these regions yield signals that are detectable.

6 Positrons

Positrons, as antiprotons that we shall describe in the following, present the complication of propagating throughout the Intergalactic Medium. Numerous treatments, making a different set of assumptions and simplifications have been presented in the literature [73, 74, 75] and applied in the case of the MSSM [76, 77, 78, 79]. Here we shall use the two-zone diffusion model and its semi-analytical solution as described in reference [75]. In this model, positron and antiproton propagation takes place in a cylindrical region (Diffusive Zone, DZ) around the galactic center of half thickness L ; the propagating particles being free to escape the region, a case in which they are simply lost. The propagation is described by a diffusion-convection-reacceleration equation:

$$\partial_t \psi + \partial_z (V_c \psi) - \nabla (K \nabla \psi) - \partial_E [b(E) \psi + K_{EE}(E) \partial_E \psi] = q, \quad (19)$$

where $\psi = dn/dE$ is the space-energy density of the positrons or antiprotons, $b(E)$ is the energy loss rate, q is the source term, $V_c \approx (5 - 15)$ km/s is the convective wind velocity wiping away the positrons or antiprotons from the galactic plane,

$$K(E) = K_0 \beta \left(\frac{E}{E_0} \right)^\alpha \quad (20)$$

is the diffusion coefficient, with β being the particle's velocity, K_0 the diffusion constant, α a constant slope, E the kinetic energy (for positrons in practice the total one), E_0 a reference energy (which we take to be 1 GeV), and

$$K_{EE} = \frac{2}{9} V_a^2 \frac{E^2 \beta^4}{K(E)} \quad (21)$$

is a coefficient describing reacceleration processes.

This is the master equation governing the propagation of cosmic rays throughout the galactic medium, which we shall be employing in the following for both positrons and antiprotons, with the details varying, of course, according to each species (e^+ or \bar{p}).

6.1 Differential event rate

It has been pointed out in the literature that the convective wind as well as reacceleration processes can be quite safely neglected for the case of positrons [80] (at least to a level sufficient for our purposes). On the other hand, energy losses should be taken into account, the most important contributions coming from synchrotron radiation or inverse Compton scattering on stellar light and CMB photons. To account for these two processes, we write the energy loss rate as:

$$b(E) = \frac{E^2}{E_0 \tau_E}, \quad (22)$$

where E is the positron energy and $\tau_E = 10^{16}$ s is the characteristic energy-loss time. We are then left with the following equation:

$$\partial_t \psi - \nabla [K(\vec{x}, E) \nabla \psi] - \partial_E [b(E) \psi] = q(\vec{x}, E), \quad (23)$$

	L [kpc]	K_0 [kpc ² /Myr]	α
MIN	1	0.00595	0.55
MED	4	0.0112	0.70
MAX	15	0.0765	0.46

Table 2: Values of propagation parameters widely used in the literature and that roughly provide minimal and maximal positron fluxes, or constitute the best fit to the B/C data.

where K is the space diffusion coefficient –steady state is assumed. This coefficient is taken to be constant in space but depends on the energy as

$$K(E) = K_0 \left(\frac{E}{E_0} \right)^\alpha. \quad (24)$$

Here the diffusion constant, K_0 , and the spectral index, α , are propagation parameters. Regarding the propagation parameters L , K_0 and α , we take their values from the commonly used MIN, MAX and MED models –see table 2. The former two models correspond to the minimal and maximal positron fluxes that are compatible with the B/C data [81]. The MED model, on the other hand, corresponds to the parameters that best fit the B/C data.

The master equation for positron propagation (equation (23)) gets simplified to its final form

$$K_0 \epsilon^\alpha \nabla^2 \psi + \frac{\partial}{\partial \epsilon} \left(\frac{\epsilon^2}{\tau_E} \psi \right) + q = 0, \quad (25)$$

where $\epsilon \equiv E/E_0$. This is the expression we solve to calculate the effects of positron propagation on a signal produced at some point in the galaxy.

The resulting positron flux from DM annihilations can be written as (see reference [73, 75] for details)

$$\Phi_{e^+}(E) = \frac{\beta_{e^+} \langle \sigma v \rangle}{4\pi} \frac{1}{2} \left(\frac{\rho(\vec{x}_\odot)}{m_\chi} \right)^2 \frac{\tau_E}{E^2} \int_E^{m_\chi} f(E_s) \tilde{I}(\lambda_D) dE_s, \quad (26)$$

where the detection and the production energy are denoted respectively by E and E_s , \vec{x}_\odot is the solar position with respect to the GC and β_{e^+} is the positron velocity. $f(E_s)$ is the production spectrum for positrons, $f(E_s) = \sum_i dN_{e^+}^i/dE_s$, with i running over all possible annihilation channels. The diffusion length, λ_D , is defined by

$$\lambda_D^2 = 4 K_0 \tau_E \left(\frac{\epsilon^{\alpha-1} - \epsilon_s^{\alpha-1}}{1 - \alpha} \right). \quad (27)$$

The so-called halo function, \tilde{I} , contains all the dependence on astrophysical factors. It is given by

$$\tilde{I}(\lambda_D) = \int_{DZ} d^3 \vec{x}_s \tilde{G}(\vec{x}_\odot, E \rightarrow \vec{x}_s, E_s) \left(\frac{\rho(\vec{x}_s)}{\rho(\vec{x}_\odot)} \right)^2, \quad (28)$$

where the integral is performed over the diffusion zone. The modified Green function \tilde{G} is in its turn defined by

$$\tilde{G} = \frac{1}{4\pi K_0 \tilde{\tau}} e^{-(r_\odot - r_s)^2 / (4K_0 \tilde{\tau})} \tilde{V}, \quad (29)$$

with \tilde{V} depending on the value of the characteristic parameter $\zeta = \frac{L^2}{4K_0\tilde{\tau}}$ and $\tilde{\tau} = \tilde{t} - \tilde{t}_s = \tau_E [(\epsilon^{\alpha-1}/(1-\alpha)) - (\epsilon_s^{\alpha-1}/(1-\alpha))]$. When $\zeta > 1$ –when the diffusion time is small– boundary conditions can be ignored and the propagation equation can be treated as a 1D Schrödinger equation. In that case

$$\tilde{V} = \frac{1}{\sqrt{4\pi K_0 \tilde{\tau}}} \exp\left[-\frac{(z_\odot - z_s)^2}{4K_0 \tilde{\tau}}\right]. \quad (30)$$

When ζ is small this approximation no longer holds but we can express \tilde{V} as

$$\tilde{V} = \sum_{n=1}^{\infty} \frac{1}{L} \left[e^{-\lambda_n \tilde{\tau}} \phi_n(z_s) \phi_n(z_\odot) + e^{-\lambda'_n \tilde{\tau}} \phi'_n(z_s) \phi'_n(z_\odot) \right] \quad (31)$$

where

$$\phi_n(z) = \sin[k_n(L - |z|)], \quad k_n = \left(n - \frac{1}{2}\right) \frac{\pi}{L}, \quad (32)$$

$$\phi'_n(z) = \sin[k'_n(L - z)], \quad k'_n = n \frac{\pi}{L}, \quad (33)$$

$\lambda_n = K_0 k_n^2$ and $\lambda'_n = K_0 (k'_n)^2$.

The advantage of this method is that the halo function $\tilde{I}(\lambda_D)$ can be calculated (and either tabulated or fitted) just once as a function of the diffusion length and then be easily used for performing parameter space scans which, as in our case, can be rather large.

Let us however note, and this shall also be the case for antiprotons, that this method has been proved to have a limited validity. More specifically, at energies below 10 GeV, some of the assumptions and simplifications that we made no longer hold. For this reason we shall limit ourselves at energies ≥ 10 GeV.

6.2 The background

In the conventional background model [82], positrons are produced in the interactions between cosmic-ray nuclei and the interstellar medium (ISM). This model is however not compatible with the recent data from PAMELA [83] and Fermi-LAT [84].

Even after taking into account several possible uncertainties due to cosmic ray propagation, the data reveals a clear excess over this background at high energies, $E \gtrsim 10$ GeV. Hence, a new source of high energy positrons is necessary to explain the data. It also turns out to be exceedingly difficult to reconcile the observed excess with dark matter annihilations. A large number of models trying to do so have been proposed in the literature, most of which turn out to be in conflict with other observational data (see, e.g. the interesting treatments in references [85, 86, 87, 88, 89, 90, 91, 92, 93, 94, 95, 96, 97]).

Although obviously dark matter annihilation could, in principle, account at least for some part of the observed excess, we feel that the most conservative choice is to consider the whole PAMELA signal as been due to some -yet unknown- astrophysical process, such as a pulsar [98, 99, 100] and treat it as a background for the oncoming AMS-02 experiment [101]. We shall use as a background the absolute positron flux that can be obtained through a combination of the PAMELA and Fermi data.

6.3 AMS-02 and positron detection

The scheduled AMS-02 mission aims at the detection and measurement of cosmic-ray fluxes (and also γ -rays) coming from various sources. Among these sources could, of course, be dark matter annihilations.

In the case of positrons, AMS-02 will be able to measure the spectrum of positrons with an average geometrical acceptance of $0.042 \text{ m}^2 \text{ sr}$ in the energy range above 4 GeV [102]. In our study we consider a 3-year run, which is actually the collaboration's nominal run time, and an energy range extending up to 300 GeV, with 20 logarithmically evenly spaced bins.

6.4 Results

6.4.1 Correlated stop-slepton masses

The results concerning the detectability perspectives for the mSUGRA-like scenario in the positron detection channel are quite pessimistic. In fact, since the PAMELA and Fermi measurements mentioned above, and according to our conservative treatment, the main issue in the positron channel is an extreme domination of all measurements by a large background severely obscuring the signal.

Obviously, one could invoke large boost factors of an astrophysical nature as was the case in the first efforts to explain the PAMELA excess through dark matter annihilations, a case in which a larger portion of the parameter space would be visible. However, it has been pointed out that it is highly unlikely to expect large boost factors due, e.g., to substructures in the halo [103]. In this respect, if we assume a maximal clump-due signal enhancement by a factor ~ 10 , the only hope for positive detection of a non-LEP excluded area might come for the bulk region, as it is the only one lying at the limits of detectability. For the sake of brevity, we omit the relevant plots for the mSUGRA-like benchmark, since no point of the parameter space can be tested.

6.4.2 Light stops, heavy sleptons

In figure 5 we present the detection perspectives in the positron channel for our scenario with light stops and heavy sleptons. The detectable parameter space regions lie within the zones delimited by the black lines for the three propagation models: the oval-shaped blobs as well as the banana-shaped ones. Once again, we notice the general features already present in the γ -ray channel. The regions giving rise to a positive detection lie within the zone where the LSP is a higgsino-like state, with mass $m_\chi > m_W$, in order to have the final state W^+W^- kinematically available. This region in general does not fulfill the WMAP limit. However, and this is a novel feature of the BMSSM, with both ϵ_1 and ϵ_2 couplings turned on, a small region of the mixed higgsino-bino regime can be detected for the MAX (and even the MED) propagation model. As we pointed out before, in this regime the total annihilation cross-section can be quite significantly enhanced, leading to better detection perspectives.

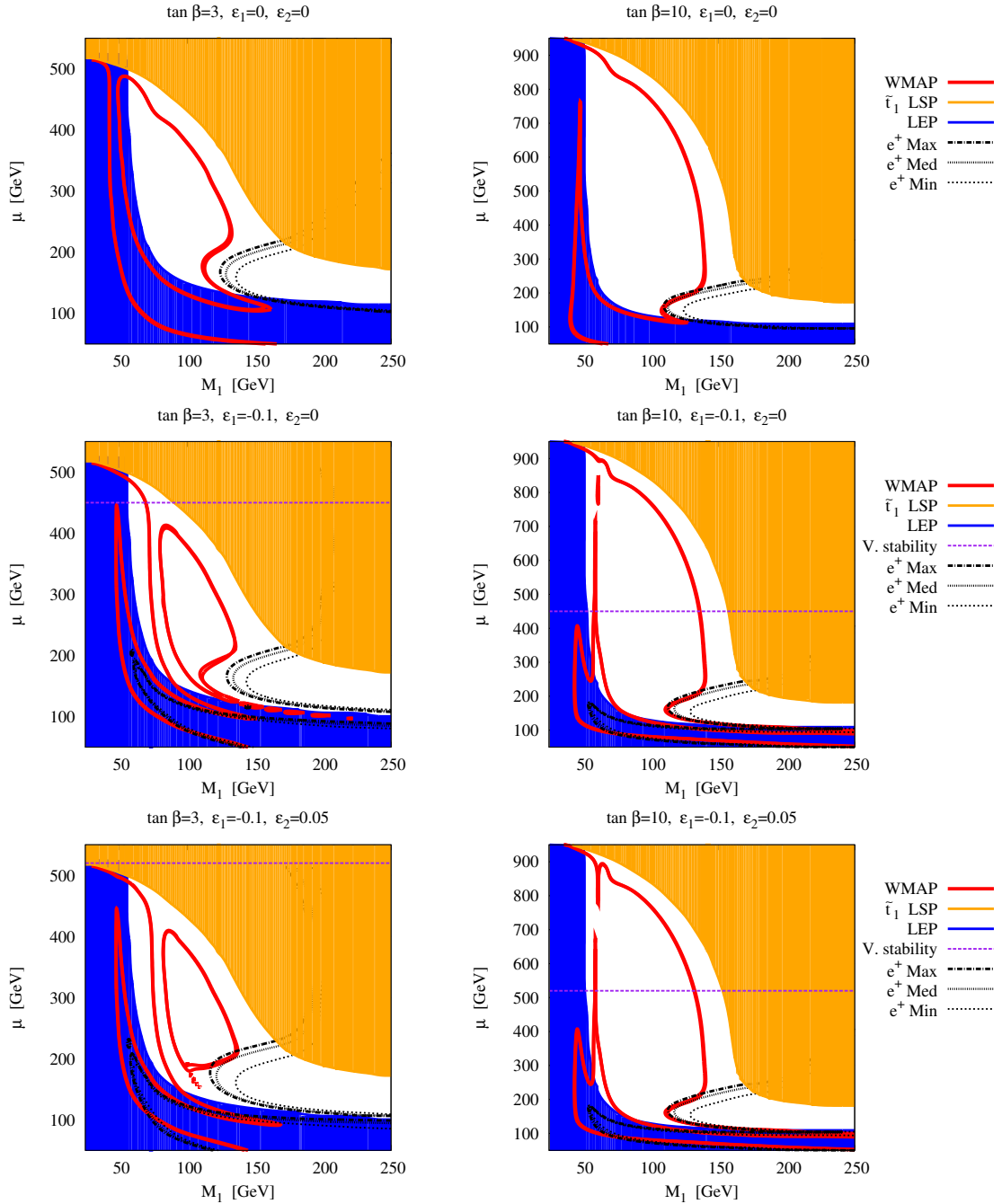


Figure 5: Regions in the $[M_1, \mu]$ plane that can be detected by a 3-year run of the AMS-02 satellite mission for the scenario with light stops and heavy sleptons, in the positron channel. The black lines depict the detectability regions for the 3 considered propagation models, MIN, MED and MAX: the parameter space points lying within the regions delimited by the black lines can be probed, assuming the corresponding propagation models. Part of the mixed bino-higgsino region, as well as (marginally) some part of the Z funnel region can be probed.

7 Antiprotons

7.1 Differential Event Rate

Equation (19) also governs antiproton propagation in the galactic medium. Nevertheless, the dominant processes vary significantly with respect to the positron case. More precisely, all energy redistributions in the initial (injection) spectrum –energy losses, reacceleration, as well as ‘tertiary’ contributions (i.e. contributions from secondary antiprotons produced upon inelastic scattering with the interstellar medium)– can be ignored. Whether these redistributions are important or not depends mainly on the antiproton energy. For GeV energies, the results may deviate up to 50% from those obtained with the (more complete) Bessel function treatment¹. But for energies around 10 GeV, the accuracy of the method improves dramatically, yielding essentially indistinguishable results at slightly higher energies. Since the \bar{p} energy region we shall consider begins at 10 GeV, we can safely use this simplified approach.

Let us denote by $\Gamma_{\bar{p}}^{\text{ann}} = \sum_{\text{ISM}} n_{\text{ISM}} v \sigma_{\bar{p} \text{ ISM}}^{\text{ann}}$ the destruction rate of antiprotons in the interstellar medium, where ISM = H and He, n_{ISM} is the average number density of ISM in the galactic disk, v is the antiproton velocity and $\sigma_{\bar{p} \text{ ISM}}^{\text{ann}}$ is the \bar{p} – ISM annihilation cross-section. Implementing the aforementioned simplifications, the transport equation for a point source (which actually defines the propagator G) is:

$$\left[-K \nabla + V_c \frac{\partial}{\partial z} + 2h \Gamma_{\bar{p}}^{\text{ann}} \delta(z) \right] G = \delta(\vec{r} - \vec{r}'), \quad (34)$$

with $h = 100$ pc being the half-thickness of the galactic disc. The antiproton propagator at the solar position can then be written (in cylindrical coordinates) as

$$G_{\bar{p}}^{\odot}(r, z) = \frac{e^{-k_v z}}{2\pi K L} \sum_{n=0}^{\infty} c_n^{-1} K_0\left(r \sqrt{k_n^2 + k_v^2}\right) \sin(k_n L) \sin(k_n (L - z)), \quad (35)$$

where K_0 is a modified Bessel function of the second kind and

$$c_n = 1 - \frac{\sin(k_n L) \cos(k_n L)}{k_n L}, \quad (36)$$

$$k_v = V_c / (2K), \quad (37)$$

$$k_d = 2h \Gamma_{\bar{p}}^{\text{ann}} / K + 2k_v. \quad (38)$$

k_n is obtained as the solution of the equation

$$n\pi - k_n L - \arctan(2k_n/k_d) = 0, \quad n \in \mathbb{N}. \quad (39)$$

Then, in order to compute the flux expected on earth, we should convolute the Green function (35) with the source distribution $q(\vec{x}, E)$. For dark matter annihilations in the galactic halo, the source term is given by

$$q(\vec{x}, E) = \frac{1}{2} \left(\frac{\rho(\vec{x})}{m_\chi} \right)^2 \sum_i \left(\langle \sigma v \rangle \frac{dN_{\bar{p}}^i}{dE_{\bar{p}}} \right), \quad (40)$$

¹In reference [104] a comparison between the two methods can be found (see figure 2).

	L [kpc]	K_0 [kpc ² /Myr]	α	V_c [km/s]
MIN	1	0.0016	0.85	13.5
MED	4	0.0112	0.70	12.0
MAX	15	0.0765	0.46	5.0

Table 3: Values of propagation parameters widely used in the literature and that provide minimal and maximal antiproton fluxes, or constitute the best fit to the B/C data.

where the index i runs over all possible annihilation final states. As in the previous cases, the decay of SM particles into antiprotons has been calculated with PYTHIA [51]. Regarding the distribution of dark matter in the Galaxy, $\rho(\vec{x})$, we assume a NFW profile. The final expression for the antiproton flux on the Earth takes the form

$$\Phi_{\odot}^{\bar{p}}(E_{\text{kin}}) = \frac{c\beta}{4\pi} \frac{\langle\sigma v\rangle}{2} \left(\frac{\rho(\vec{x}_{\odot})}{m_{\chi}}\right)^2 \frac{dN}{dE}(E_{\text{kin}}) \int_{DZ} \left(\frac{\rho(\vec{x}_s)}{\rho(\vec{x}_{\odot})}\right)^2 G_{\bar{p}}^{\odot}(\vec{x}_s) d^3x, \quad (41)$$

where none of the integrated quantities depends on the antiproton energy. Once again, the integral in equation (41), which we compute using a VEGAS Monte-Carlo algorithm, needs to be calculated only once for each value of the injection energy, which is actually the same as the detection energy.

Regarding the propagation parameters L , K_0 , α , and V_c , we take their values from the well-established MIN, MAX and MED models –see table 3. The former two models correspond to the minimal and maximal antiprotons fluxes that are compatible with the B/C data. The MED model, on the other hand, corresponds to the parameters that best fit the B/C data.

7.2 The background

Contrary to the positron case, the most well-known treatment of the astrophysical antiproton background by Strong and Moskalenko [105], seems to be compatible with the antiproton data [106] from the PAMELA experiment.

In order to parametrize our background, we borrow the simple fit performed by Cirelli *et al.* [107], which provides a sufficiently good fit for our purposes, to theoretical predictions but also to the recent PAMELA data. We pay special attention at reproducing the good background normalization at low energies, so as to stay as close as possible to the PAMELA measurements.

7.3 AMS-02 and antiproton detection

In the case of antiprotons, AMS-02 will be able to measure [102] the corresponding fluxes with an average geometrical acceptance of 330 cm² sr above 16 GeV and up to 300 GeV. In our study we again consider a 3-year run and the mentioned energy range divided into 20 logarithmically evenly spaced energy bins.

7.4 Results

7.4.1 Correlated stop-slepton masses

In figure 6 we present our results for the detectability of the BMSSM in comparison to the MSSM by the AMS-02 experiment for the antiproton channel. The detectable regions lie below the black lines. In the case $\tan\beta = 3$, the experiment is not sensitive to any point in the parameter space satisfying

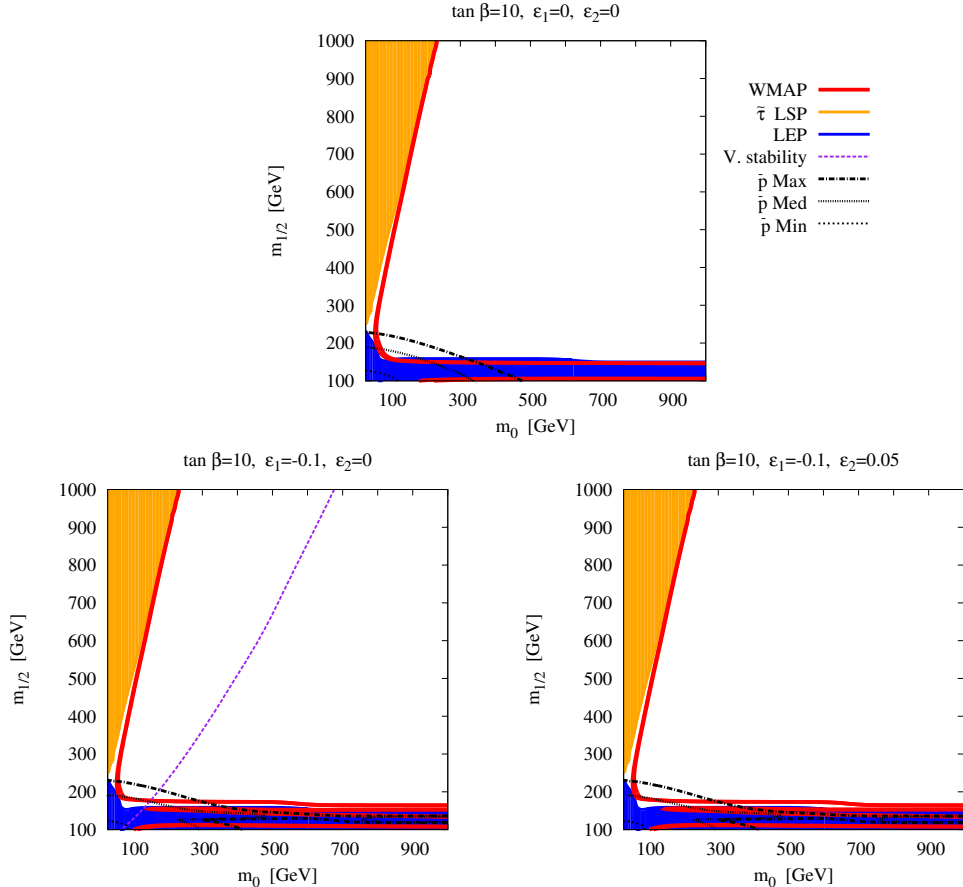


Figure 6: Regions in the $[m_0, m_{1/2}]$ plane that can be detected by a 3-year run of the AMS-02 satellite mission for our mSUGRA-like scenario in the antiproton channel. The black lines depict the detectability regions for the 3 considered propagation models: the area delimited by the axes and the black lines can be probed for the corresponding propagation model (i.e. the region towards the lower left corner in each plot).

also the collider constraints (and, hence, the corresponding results are once again omitted). A first remark here should concern the fact that the perspectives for antiproton detection are significantly ameliorated with respect to the corresponding positron ones, at least for large values of $\tan\beta$. This could, in some sense, seem quite strange, since the average antiproton yield coming from a DM annihilation is, in general, smaller than the positron one. However, we should take into account that these results reflect not only the behaviour of the models themselves, but also the interplay between the signal and the background. And, as it turns out the \bar{p} channel is a significantly low-background

one.

Important areas of the viable parameter space are at the limits of detectability: the bulk region, but also, for some cases, the Higgs funnel. Now, as we stressed out before, the possible enhancements due for example to substructures are quite constrained. Given however that some regions are marginally out of reach, it would not be impossible to state that even small boosts could render important (in a qualitative sense, due to their cosmological relevance) regions of the parameter space detectable by AMS-02.

7.4.2 Light stops, heavy sleptons

Figure 7 presents the results for antiprotons and for the second scenario under consideration. AMS-02 will be able to probe the regions lying within the oval-like blobs and the banana-shaped regions delimited by the black contours and the axes. Once again, the BMSSM turns out to be more favorable for DM detection than the ordinary case of light stops and heavy sleptons without NR operators. Detectable regions fall either into the case of the higgsino-like neutralino regime, or in the low-mass Z funnel region. We point out that an important part of the area where the dark matter relic density is fulfilled via coannihilation with the lightest stop could also be tested.

8 Conclusions

In this paper, we presented detection perspectives for neutralino dark matter in the framework of the so-called BMSSM, where the superpotential is enriched by the addition of dimension-5 non-renormalizable operators in the Higgs sector. The main motivation to add non-renormalizable operators to the MSSM Higgs sector is to reduce the fine-tuning that is required by the lower bound on the Higgs mass. These new terms re-open the bulk region, already excluded because it gives rise to a too light Higgs boson. Focusing on the new available regions, we have studied four of the most popular detection modes: direct detection, as well as three different channels of indirect detection, γ -rays from the galactic center, positrons and antiprotons. We placed ourselves in the framework of the experiments XENON, Fermi and AMS-02.

According to our results, the most favourable detection mode seems to be, by far, the direct one. XENON, even for low exposures, can provide a sizable parameter space coverage and, in case of a negative detection, can exclude a significant part of the model. Moreover, regions of the supersymmetric parameter space that were favored by the WMAP constraint, but were excluded within the MSSM, become viable within the BMSSM and could be potentially detected.

From the indirect detection point of view, we have shown that gamma-rays are the most favoured probe in the benchmarks of the BMSSM we examined. We stress nevertheless that this is the case assuming quite optimistic astrophysical conditions, namely an important collapse of dark matter in the galactic center due to the presence of baryons, yielding a significantly spiked inner region profile. We should also note again that we considered a 5-year Fermi mission, whereas a period of 3 years was considered for the AMS-02 experiment. On the other hand, antiprotons can provide significant information without having to assume extreme conditions for the galactic medium: we

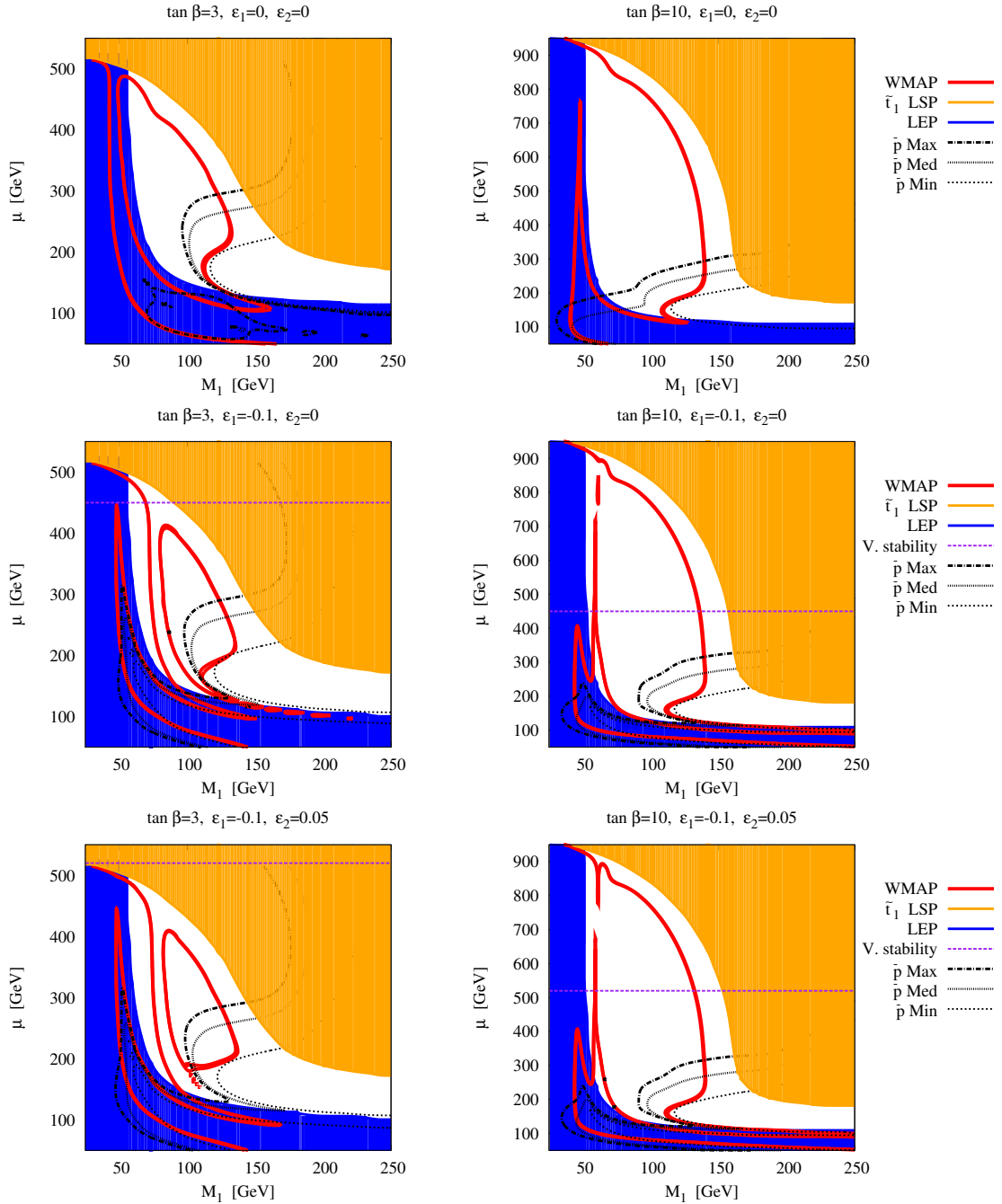


Figure 7: Regions in the $[M_1, \mu]$ plane that can be detected by a 3-year run of the AMS-02 satellite mission for the scenario with light stops and heavy sleptons, in the antiproton channel. The black lines depict the detectability regions for the 3 considered propagation models: the areas delimited by the axes and the black lines can be probed for the corresponding propagation model (i.e. the regions towards the lower right side in each plot), as well as the areas delimited by closed lines.

only used the standard propagation models used in numerous other analyses in the literature. However, the detection prospects could be enhanced taking into account DM substructures, which

could provide a -small- amelioration of the signals by at most one order of magnitude. For positrons, our treatment for the background seems to lead us to conclude that the PAMELA data, providing a large supplementary background with respect to previous estimates, seem to render a positive detection in this channel more difficult.

As a final remark, it is interesting to note again that for the low $\tan\beta$ values we considered here, as we wanted to stick to the original motivation for the model (uplifting the Higgs mass without over-constraining the stop sector), direct detection seems dominant. It is quite well-known that increasing $\tan\beta$ usually tends to ameliorate the indirect detection prospects, contrary to direct detection ones. This is an element which can give us an idea of the complementarity of the various detection modes. As underlined in [46, 91], different detection techniques offer the possibility for a more complete parameter space coverage. Moreover, they can serve as a means for independent confirmation of discoveries and/or comparison with other constraints. Given the controversy that has been generated during the past few years on the nature of the various excesses that have occasionally been observed, we feel that combining information from various sources is an essential element in our searches.

Acknowledgements

The authors would like to thank G. Bélanger for useful discussions about the implementation of the model in micrOMEGAs. AG would like to acknowledge enlightening discussions with F. Bonnet, M. Fornasa, M. Gustafsson, M. Pato and M. Passera. We would like to thank Y. Mambrini and S. Palomares-Ruiz for careful reading of the manuscript and valuable remarks. The work of NB and AG is supported in part by the E.C. Research Training Networks under contract MRTN-CT-2006-035505. AG is also supported by the french ANR TAPDMS.

References

- [1] A. Djouadi, “The Anatomy of electro-weak symmetry breaking. II. The Higgs bosons in the minimal supersymmetric model”, *Phys. Rept.* **459** (2008) 1–241, [arXiv:hep-ph/0503173](#).
- [2] A. Strumia, “Bounds on Kaluza-Klein excitations of the SM vector bosons from electroweak tests”, *Phys. Lett.* **B466** (1999) 107–114, [arXiv:hep-ph/9906266](#).
- [3] A. Brignole, J. A. Casas, J. R. Espinosa, and I. Navarro, “Low-scale supersymmetry breaking: Effective description, electroweak breaking and phenomenology”, *Nucl. Phys.* **B666** (2003) 105–143, [arXiv:hep-ph/0301121](#).
- [4] J. A. Casas, J. R. Espinosa, and I. Hidalgo, “The MSSM fine tuning problem: A Way out”, *JHEP* **01** (2004) 008, [arXiv:hep-ph/0310137](#).
- [5] M. Pospelov, A. Ritz, and Y. Santoso, “Flavor and CP violating physics from new supersymmetric thresholds”, *Phys. Rev. Lett.* **96** (2006) 091801, [arXiv:hep-ph/0510254](#).

- [6] M. Pospelov, A. Ritz, and Y. Santoso, “Sensitivity to new supersymmetric thresholds through flavour and CP violating physics”, *Phys. Rev.* **D74** (2006) 075006, [arXiv:hep-ph/0608269](https://arxiv.org/abs/hep-ph/0608269).
- [7] M. Dine, N. Seiberg, and S. Thomas, “Higgs Physics as a Window Beyond the MSSM (BMSSM)”, *Phys. Rev.* **D76** (2007) 095004, [arXiv:0707.0005](https://arxiv.org/abs/hep-ph/0707.0005) [hep-ph].
- [8] P. Batra and E. Pontón, “Supersymmetric electroweak symmetry breaking”, *Phys. Rev.* **D79** (2009) 035001, [arXiv:0809.3453](https://arxiv.org/abs/hep-ph/0809.3453) [hep-ph].
- [9] I. Antoniadis, E. Dudas, D. M. Ghilencea, and P. Tziveloglou, “MSSM with Dimension-five Operators (MSSM₅)”, *Nucl. Phys.* **B808** (2009) 155–184, [arXiv:0806.3778](https://arxiv.org/abs/hep-ph/0806.3778) [hep-ph].
- [10] I. Antoniadis, E. Dudas, D. M. Ghilencea, and P. Tziveloglou, “MSSM Higgs with dimension-six operators”, [arXiv:0910.1100](https://arxiv.org/abs/hep-ph/0910.1100) [hep-ph].
- [11] K. Blum, C. Delaunay, and Y. Hochberg, “Vacuum (Meta)Stability Beyond the MSSM”, *Phys. Rev.* **D80** (2009) 075004, [arXiv:0905.1701](https://arxiv.org/abs/hep-ph/0905.1701) [hep-ph].
- [12] K. Blum and Y. Nir, “Beyond MSSM Baryogenesis”, *Phys. Rev.* **D78** (2008) 035005, [arXiv:0805.0097](https://arxiv.org/abs/hep-ph/0805.0097) [hep-ph].
- [13] N. Bernal, K. Blum, Y. Nir, and M. Losada, “BMSSM Implications for Cosmology”, *JHEP* **08** (2009) 053, [arXiv:0906.4696](https://arxiv.org/abs/hep-ph/0906.4696) [hep-ph].
- [14] K. Cheung, S. Y. Choi, and J. Song, “Impact on the Light Higgsino-LSP Scenario from Physics beyond the Minimal Supersymmetric Standard Model”, *Phys. Lett.* **B677** (2009) 54–58, [arXiv:0903.3175](https://arxiv.org/abs/hep-ph/0903.3175) [hep-ph].
- [15] M. Berg, J. Edsjö, P. Gondolo, E. Lundstrom, and S. Sjors, “Neutralino Dark Matter in BMSSM Effective Theory”, *JCAP* **0908** (2009) 035, [arXiv:0906.0583](https://arxiv.org/abs/hep-ph/0906.0583) [hep-ph].
- [16] M. Carena, K. Kong, E. Pontón, and J. Zurita, “Supersymmetric Higgs Bosons and Beyond”, [arXiv:0909.5434](https://arxiv.org/abs/hep-ph/0909.5434) [hep-ph].
- [17] S. Cassel, D. M. Ghilencea, and G. G. Ross, “Fine tuning as an indication of physics beyond the MSSM”, *Nucl. Phys.* **B825** (2010) 203–221, [arXiv:0903.1115](https://arxiv.org/abs/hep-ph/0903.1115) [hep-ph].
- [18] <http://fermi.gsfc.nasa.gov/>.
- [19] <http://ams.cern.ch>.
- [20] S. Davidson, T. Falk, and M. Losada, “Dark matter abundance and electroweak baryogenesis in the CMSSM”, *Phys. Lett.* **B463** (1999) 214–224, [arXiv:hep-ph/9907365](https://arxiv.org/abs/hep-ph/9907365).
- [21] C. Balázs, M. S. Carena, and C. E. M. Wagner, “Dark matter, light stops and electroweak baryogenesis”, *Phys. Rev.* **D70** (2004) 015007, [arXiv:hep-ph/0403224](https://arxiv.org/abs/hep-ph/0403224).

- [22] G. Bélanger, F. Boudjema, A. Pukhov, and A. Semenov, “micrOMEGAs2.0: A program to calculate the relic density of dark matter in a generic model”, *Comput. Phys. Commun.* **176** (2007) 367–382, [arXiv:hep-ph/0607059](#).
- [23] G. Bélanger, F. Boudjema, A. Pukhov, and A. Semenov, “Dark matter direct detection rate in a generic model with micrOMEGAs2.2”, *Comput. Phys. Commun.* **180** (2009) 747–767, [arXiv:0803.2360 \[hep-ph\]](#).
- [24] A. Djouadi, J.-L. Kneur, and G. Moultaka, “SuSpect: A Fortran code for the supersymmetric and Higgs particle spectrum in the MSSM”, *Comput. Phys. Commun.* **176** (2007) 426–455, [arXiv:hep-ph/0211331](#).
- [25] A. H. Chamseddine, R. L. Arnowitt, and P. Nath, “Locally Supersymmetric Grand Unification”, *Phys. Rev. Lett.* **49** (1982) 970.
- [26] R. Barbieri, S. Ferrara, and C. A. Savoy, “Gauge Models with Spontaneously Broken Local Supersymmetry”, *Phys. Lett.* **B119** (1982) 343.
- [27] L. J. Hall, J. D. Lykken, and S. Weinberg, “Supergravity as the Messenger of Supersymmetry Breaking”, *Phys. Rev.* **D27** (1983) 2359–2378.
- [28] N. Ohta, “Grand unified theories based on local supersymmetry”, *Prog. Theor. Phys.* **70** (1983) 542.
- [29] A. Belyaev, S. Dar, I. Gogoladze, A. Mustafayev, and Q. Shafi, “Interplay of Higgs and Sparticle Masses in the CMSSM with updated SUSY constraints”, [arXiv:0712.1049 \[hep-ph\]](#).
- [30] **WMAP** Collaboration, J. Dunkley *et al.*, “Five-Year Wilkinson Microwave Anisotropy Probe (WMAP) Observations: Likelihoods and Parameters from the WMAP data”, *Astrophys. J. Suppl.* **180** (2009) 306–329, [arXiv:0803.0586 \[astro-ph\]](#).
- [31] A. Djouadi, M. Drees, and J.-L. Kneur, “Neutralino dark matter in mSUGRA: Reopening the light Higgs pole window”, *Phys. Lett.* **B624** (2005) 60–69, [arXiv:hep-ph/0504090](#).
- [32] **Particle Data Group** Collaboration, C. Amsler *et al.*, “Review of particle physics”, *Phys. Lett.* **B667** (2008) 1.
- [33] N. Arkani-Hamed, A. Delgado, and G. F. Giudice, “The well-tempered neutralino”, *Nucl. Phys.* **B741** (2006) 108–130, [arXiv:hep-ph/0601041](#).
- [34] K. Griest and D. Seckel, “Three exceptions in the calculation of relic abundances”, *Phys. Rev.* **D43** (1991) 3191–3203.
- [35] C. Boehm, A. Djouadi, and M. Drees, “Light scalar top quarks and supersymmetric dark matter”, *Phys. Rev.* **D62** (2000) 035012, [arXiv:hep-ph/9911496](#).

- [36] J. R. Ellis, K. A. Olive, and Y. Santoso, “Calculations of Neutralino-Stop Coannihilation in the CMSSM”, *Astropart. Phys.* **18** (2003) 395–432, [arXiv:hep-ph/0112113](#).
- [37] D. G. Cerdeño, S. Khalil, and C. Muñoz, “Supersymmetric dark matter and neutralino nucleon cross section”, [arXiv:hep-ph/0105180](#).
- [38] S. Baek, D. G. Cerdeño, Y. G. Kim, P. Ko, and C. Muñoz, “Direct detection of neutralino dark matter in supergravity”, *JHEP* **06** (2005) 017, [arXiv:hep-ph/0505019](#).
- [39] J. R. Ellis, K. A. Olive, Y. Santoso, and V. C. Spanos, “Update on the direct detection of supersymmetric dark matter”, *Phys. Rev.* **D71** (2005) 095007, [arXiv:hep-ph/0502001](#).
- [40] R. Catena and P. Ullio, “A novel determination of the local dark matter density”, [arXiv:0907.0018 \[astro-ph.CO\]](#).
- [41] M. Kuhlen *et al.*, “Dark Matter Direct Detection with Non-Maxwellian Velocity Structure”, [arXiv:0912.2358 \[astro-ph.GA\]](#).
- [42] G. Jungman, M. Kamionkowski, and K. Griest, “Supersymmetric dark matter”, *Phys. Rept.* **267** (1996) 195–373, [hep-ph/9506380](#).
- [43] J. Engel, “Nuclear form-factors for the scattering of weakly interacting massive particles”, *Phys. Lett.* **B264** (1991) 114–119.
- [44] J. R. Ellis, K. A. Olive, and C. Savage, “Hadronic Uncertainties in the Elastic Scattering of Supersymmetric Dark Matter”, *Phys. Rev.* **D77** (2008) 065026, [arXiv:0801.3656 \[hep-ph\]](#).
- [45] **XENON** Collaboration, J. Angle *et al.*, “First Results from the XENON10 Dark Matter Experiment at the Gran Sasso National Laboratory”, *Phys. Rev. Lett.* **100** (2008) 021303, [arXiv:0706.0039 \[astro-ph\]](#).
- [46] N. Bernal, A. Goudelis, Y. Mambrini, and C. Muñoz, “Determining the WIMP mass using the complementarity between direct and indirect searches and the ILC”, *JCAP* **0901** (2009) 046, [arXiv:0804.1976 \[hep-ph\]](#).
- [47] A. M. Green, “Determining the WIMP mass from a single direct detection experiment, a more detailed study”, *JCAP* **0807** (2008) 005, [arXiv:0805.1704 \[hep-ph\]](#).
- [48] T. Bruch and f. t. C. Collaboration, “CDMS-II to SuperCDMS: WIMP search at a zeptobarn”, [arXiv:1001.3037 \[astro-ph.IM\]](#).
- [49] S. Fiorucci *et al.*, “Status of the LUX Dark Matter Search”, [arXiv:0912.0482 \[astro-ph.CO\]](#).
- [50] **The CDMS** Collaboration, Z. Ahmed *et al.*, “Results from the Final Exposure of the CDMS II Experiment”, [arXiv:0912.3592 \[astro-ph.CO\]](#).

- [51] T. Sjöstrand, S. Mrenna, and P. Skands, “PYTHIA 6.4 Physics and Manual”, *JHEP* **05** (2006) 026, [arXiv:hep-ph/0603175](#).
- [52] L. Bergström, P. Ullio, and J. H. Buckley, “Observability of gamma rays from dark matter neutralino annihilations in the Milky Way halo”, *Astropart. Phys.* **9** (1998) 137–162, [arXiv:astro-ph/9712318](#).
- [53] H. Yuksel, S. Horiuchi, J. F. Beacom, and S. Ando, “Neutrino Constraints on the Dark Matter Total Annihilation Cross Section”, *Phys. Rev.* **D76** (2007) 123506, [arXiv:0707.0196 \[astro-ph\]](#).
- [54] A. W. Graham, D. Merritt, B. Moore, J. Diemand, and B. Terzic, “Empirical models for Dark Matter Halos. I.”, *Astron. J.* **132** (2006) 2685, [arXiv:astro-ph/0509417](#).
- [55] A. W. Graham, D. Merritt, B. Moore, J. Diemand, and B. Terzic, “Empirical Models for Dark Matter Halos. II.”, *Astron. J.* **132** (2006) 2701, [arXiv:astro-ph/0608613](#).
- [56] A. W. Graham, D. Merritt, B. Moore, J. Diemand, and B. Terzic, “Empirical Models for Dark Matter Halos. III. ”, *Astron. J.* **132** (2006) 2711, [arXiv:astro-ph/0608614](#).
- [57] B. Moore *et al.*, “Dark matter substructure within galactic halos”, *Astrophys. J.* **524** (1999) L19–L22.
- [58] J. F. Navarro, C. S. Frenk, and S. D. M. White, “The Structure of Cold Dark Matter Halos”, *Astrophys. J.* **462** (1996) 563–575, [arXiv:astro-ph/9508025](#).
- [59] J. Diemand *et al.*, “Clumps and streams in the local dark matter distribution”, *Nature* **454** (2008) 735–738, [arXiv:0805.1244 \[astro-ph\]](#).
- [60] V. Springel *et al.*, “The Aquarius Project: the subhalos of galactic halos”, *Mon. Not. Roy. Astron. Soc.* **391** (2008) 1685–1711, [arXiv:0809.0898 \[astro-ph\]](#).
- [61] J. Einasto, “Influence of the atmospheric and instrumental dispersion on the brightness distribution in a galaxy”, *Trudy Inst. Astrofiz. Alma-Ata* **5** (1965) 87.
- [62] F. Prada, A. Klypin, J. Flix, M. Martínez, and E. Simonneau, “Astrophysical inputs on the SUSY dark matter annihilation detectability”, *Phys. Rev. Lett.* **93** (2004) 241301, [arXiv:astro-ph/0401512](#).
- [63] Y. Mambrini, C. Muñoz, E. Nezri, and F. Prada, “Adiabatic compression and indirect detection of supersymmetric dark matter”, *JCAP* **0601** (2006) 010, [arXiv:hep-ph/0506204](#).
- [64] L. Bergström, J. Edsjö, P. Gondolo, and P. Ullio, “Clumpy neutralino dark matter”, *Phys. Rev.* **D59** (1999) 043506, [arXiv:astro-ph/9806072](#).

- [65] **The HESS** Collaboration, F. Aharonian *et al.*, “Very high energy gamma rays from the direction of Sagittarius A*”, *Astron. Astrophys.* **425** (2004) L13–L17, [arXiv:astro-ph/0408145](#).
- [66] S. Profumo, “TeV gamma-rays and the largest masses and annihilation cross sections of neutralino dark matter”, *Phys. Rev.* **D72** (2005) 103521, [arXiv:astro-ph/0508628](#).
- [67] F. Aharonian and A. Neronov, “High energy gamma rays from the massive black hole in the galactic center”, *Astrophys. J.* **619** (2005) 306–313, [arXiv:astro-ph/0408303](#).
- [68] S. D. Hunter *et al.*, “EGRET observations of the diffuse gamma-ray emission from the galactic plane”, *Astrophys. J.* **481** (1997) 205–240.
- [69] T. A. Porter and f. t. F. L. Collaboration, “Fermi LAT Measurements of the Diffuse Gamma-Ray Emission at Intermediate Galactic Latitudes”, [arXiv:0907.0294 \[astro-ph.HE\]](#).
- [70] **H.E.S.S.** Collaboration, F. Aharonian *et al.*, “Discovery of Very-High-Energy Gamma-Rays from the Galactic Centre Ridge”, *Nature* **439** (2006) 695–698, [arXiv:astro-ph/0603021](#).
- [71] N. Gehrels and P. Michelson, “GLAST: The next-generation high energy gamma-ray astronomy mission”, *Astropart. Phys.* **11** (1999) 277–282.
- [72] S. Peirani, R. Mohayaee, and J. A. de Freitas Pacheco, “Indirect search for dark matter: Prospects for GLAST”, *Phys. Rev.* **D70** (2004) 043503, [arXiv:astro-ph/0401378](#).
- [73] E. A. Baltz and J. Edsjö, “Positron Propagation and Fluxes from Neutralino Annihilation in the Halo”, *Phys. Rev.* **D59** (1998) 023511, [arXiv:astro-ph/9808243](#).
- [74] A. W. Strong and I. V. Moskalenko, “Galactic cosmic rays and gamma rays: a unified approach”, [arXiv:astro-ph/9812260](#).
- [75] J. Lavalle, J. Pochon, P. Salati, and R. Taillet, “Clumpiness of dark matter and positron annihilation signal: Computing the odds of the galactic lottery”, [arXiv:astro-ph/0603796](#).
- [76] Y. Mambrini, C. Muñoz, and E. Nezri, “A comparison between the detection of gamma rays and positrons from neutralino annihilation”, *JCAP* **0612** (2006) 003, [arXiv:hep-ph/0607266](#).
- [77] E. A. Baltz, J. Edsjö, K. Freese, and P. Gondolo, “The cosmic ray positron excess and neutralino dark matter”, *Phys. Rev.* **D65** (2002) 063511, [arXiv:astro-ph/0109318](#).
- [78] W. de Boer, C. Sander, M. Horn, and D. Kazakov, “Positron fraction from dark matter annihilation in the CMSSM”, *Nucl. Phys. Proc. Suppl.* **113** (2002) 221–228, [arXiv:astro-ph/0207557](#).

- [79] D. Hooper, A. Stebbins, and K. M. Zurek, “Excesses in cosmic ray positron and electron spectra from a nearby clump of neutralino dark matter”, *Phys. Rev.* **D79** (2009) 103513, [arXiv:0812.3202 \[hep-ph\]](#).
- [80] T. Delahaye *et al.*, “Galactic secondary positron flux at the Earth”, *Astron. Astrophys.* **501** (2009) 821–833, [arXiv:0809.5268 \[astro-ph\]](#).
- [81] T. Delahaye, R. Lineros, F. Donato, N. Fornengo, and P. Salati, “Positrons from dark matter annihilation in the galactic halo: theoretical uncertainties”, *Phys. Rev.* **D77** (2008) 063527, [arXiv:0712.2312 \[astro-ph\]](#).
- [82] A. W. Strong, I. V. Moskalenko, and O. Reimer, “Diffuse Galactic continuum gamma rays. A model compatible with EGRET data and cosmic-ray measurements”, *Astrophys. J.* **613** (2004) 962–976, [arXiv:astro-ph/0406254](#).
- [83] **PAMELA** Collaboration, O. Adriani *et al.*, “An anomalous positron abundance in cosmic rays with energies 1.5–100 GeV”, *Nature* **458** (2009) 607–609, [arXiv:0810.4995 \[astro-ph\]](#).
- [84] **The Fermi LAT** Collaboration, A. A. Abdo *et al.*, “Measurement of the Cosmic Ray e^+ plus e^- spectrum from 20 GeV to 1 TeV with the Fermi Large Area Telescope”, *Phys. Rev. Lett.* **102** (2009) 181101, [arXiv:0905.0025 \[astro-ph.HE\]](#).
- [85] M. Cirelli, M. Kadastik, M. Raidal, and A. Strumia, “Model-independent implications of the e^+ , e^- , anti-proton cosmic ray spectra on properties of Dark Matter”, *Nucl. Phys.* **B813** (2009) 1–21, [arXiv:0809.2409 \[hep-ph\]](#).
- [86] G. Bertone, M. Cirelli, A. Strumia, and M. Taoso, “Gamma-ray and radio tests of the e^+e^- excess from DM annihilations”, *JCAP* **0903** (2009) 009, [arXiv:0811.3744 \[astro-ph\]](#).
- [87] L. Bergström, G. Bertone, T. Bringmann, J. Edsjö, and M. Taoso, “Gamma-ray and Radio Constraints of High Positron Rate Dark Matter Models Annihilating into New Light Particles”, *Phys. Rev.* **D79** (2009) 081303, [arXiv:0812.3895 \[astro-ph\]](#).
- [88] I. Gogoladze, R. Khalid, Q. Shafi, and H. Yüksel, “CMSSM Spectroscopy in light of PAMELA and ATIC”, *Phys. Rev.* **D79** (2009) 055019, [arXiv:0901.0923 \[hep-ph\]](#).
- [89] M. Cirelli and P. Panci, “Inverse Compton constraints on the Dark Matter e^+e^- excesses”, *Nucl. Phys.* **B821** (2009) 399–416, [arXiv:0904.3830 \[astro-ph.CO\]](#).
- [90] S. Galli, F. Iocco, G. Bertone, and A. Melchiorri, “CMB constraints on Dark Matter models with large annihilation cross-section”, *Phys. Rev.* **D80** (2009) 023505, [arXiv:0905.0003 \[astro-ph.CO\]](#).
- [91] M. Pato, L. Pieri, and G. Bertone, “Multi-messenger constraints on the annihilating dark matter interpretation of the positron excess”, *Phys. Rev.* **D80** (2009) 103510, [arXiv:0905.0372 \[astro-ph.HE\]](#).

- [92] P. Meade, M. Papucci, A. Strumia, and T. Volansky, “Dark Matter Interpretations of the Electron/Positron Excesses after FERMI”, [arXiv:0905.0480 \[hep-ph\]](#).
- [93] S. Profumo and T. E. Jeltema, “Extragalactic Inverse Compton Light from Dark Matter Annihilation and the Pamela Positron Excess”, *JCAP* **0907** (2009) 020, [arXiv:0906.0001 \[astro-ph.CO\]](#).
- [94] G. Huetsi, A. Hektor, and M. Raidal, “Constraints on leptonically annihilating Dark Matter from reionization and extragalactic gamma background”, [arXiv:0906.4550 \[astro-ph.CO\]](#).
- [95] M. Cirelli, F. Iocco, and P. Panci, “Constraints on Dark Matter annihilations from reionization and heating of the intergalactic gas”, *JCAP* **0910** (2009) 009, [arXiv:0907.0719 \[astro-ph.CO\]](#).
- [96] M. Cirelli, P. Panci, and P. D. Serpico, “Diffuse gamma ray constraints on annihilating or decaying Dark Matter after Fermi”, [arXiv:0912.0663 \[astro-ph.CO\]](#).
- [97] M. Papucci and A. Strumia, “Robust implications on Dark Matter from the first FERMI sky gamma map”, [arXiv:0912.0742 \[hep-ph\]](#).
- [98] D. Hooper, P. Blasi, and P. D. Serpico, “Pulsars as the Sources of High Energy Cosmic Ray Positrons”, *JCAP* **0901** (2009) 025, [arXiv:0810.1527 \[astro-ph\]](#).
- [99] H. Yuksel, M. D. Kistler, and T. Stanev, “TeV Gamma Rays from Geminga and the Origin of the GeV Positron Excess”, *Phys. Rev. Lett.* **103** (2009) 051101, [arXiv:0810.2784 \[astro-ph\]](#).
- [100] S. Profumo, “Dissecting Pamela (and ATIC) with Occam’s Razor: existing, well-known Pulsars naturally account for the ‘anomalous’ Cosmic-Ray Electron and Positron Data”, [arXiv:0812.4457 \[astro-ph\]](#).
- [101] K.-Y. Choi and C. E. Yaguna, “Implications of an astrophysical interpretation of PAMELA and Fermi-LAT data for future searches of a positron signal from dark matter annihilations”, [arXiv:0906.0736 \[hep-ph\]](#).
- [102] **AMS** Collaboration, C. Goy, “Indirect search for dark matter with AMS”, *J. Phys. Conf. Ser.* **39** (2006) 185–187.
- [103] J. Lavalle, Q. Yuan, D. Maurin, and X. J. Bi, “Full Calculation of Clumpiness Boost factors for Antimatter Cosmic Rays in the light of Λ CDM N-body simulation results”, [arXiv:0709.3634 \[astro-ph\]](#).
- [104] D. Maurin, R. Taillet, and C. Combet, “Approximate formulae for exotic GCR anti-p and anti-d: Fluxes and astrophysical uncertainties”, [arXiv:astro-ph/0609522](#).

- [105] I. V. Moskalenko, A. W. Strong, J. F. Ormes, and M. S. Potgieter, “Secondary antiprotons and propagation of cosmic rays in the Galaxy and heliosphere”, *Astrophys. J.* **565** (2002) 280–296, [arXiv:astro-ph/0106567](#).
- [106] O. Adriani *et al.*, “A new measurement of the antiproton-to-proton flux ratio up to 100 GeV in the cosmic radiation”, *Phys. Rev. Lett.* **102** (2009) 051101, [arXiv:0810.4994 \[astro-ph\]](#).
- [107] M. Cirelli and A. Strumia, “Minimal Dark Matter: model and results”, *New J. Phys.* **11** (2009) 105005, [arXiv:0903.3381 \[hep-ph\]](#).